NAVAL POSTGRADUATE SCHOOL
Monterey, California

THESIS

SEMI-LAGRANGIAN, SEMI-IMPLICIT SOLUTIONS OF THE SHALLOW WATER EQUATIONS IN ONE DIMENSION

by

Kristina B. Monk

June 1989

Thesis Advisor Roger T. Williams

nclassified

curity classification of this page

REPORT DOCUMENTATION PAGE

a Report Security Classification Unclassified		1b Restrictive Markings	
a Security Classification Authority		3 Distribution Availability of Report	
b Declassification Downgrading Schedule		Approved for public release; distribution is unlimited.	
Performing Organization Report Number(s)		5 Monitoring Organization Report Number(s)	
a Name of Performing Organization Naval Postgraduate School	6b Office Symbol *(if applicable)* 35	7a Name of Monitoring Organization Naval Postgraduate School	
c Address *(city, state, and ZIP code)* Monterey, CA 93943-5000		7b Address *(city, state, and ZIP code)* Monterey, CA 93943-5000	
a Name of Funding Sponsoring Organization	8b Office Symbol *(if applicable)*	9 Procurement Instrument Identification Number	
c Address *(city, state, and ZIP code)*		10 Source of Funding Numbers	
		Program Element No	Project No / Task No / Work Unit Accession No

1 Title *(include security classification)* SEMI-LAGRANGIAN, SEMI-IMPLICIT SOLUTIONS OF THE SHALLOW WATER QUATIONS IN ONE DIMENSION

2 Personal Author(s) Kristina B. Monk

3a Type of Report	13b Time Covered	14 Date of Report *(year, month, day)*	15 Page Count
Master's Thesis	From To	June 1989	48

6 Supplementary Notation The views expressed in this thesis are those of the author and do not reflect the official policy or po-tion of the Department of Defense or the U.S. Government.

17 Cosati Codes			18 Subject Terms *(continue on reverse if necessary and identify by block number)*
ield	Group	Subgroup	Meteorology, Numerical Weather Prediction,Semi-Lagrangian

9 Abstract *(continue on reverse if necessary and identify by block number)* The semi-Lagrangian, semi-implicit method is used to model ne one dimensional shallow water system of equations with surface topography. The forecasts are compared to finite dif-rence and semi-Lagrangian, explicit forecasts. In the first experiment, a non-rotating system is considered. The semi-agrangian, semi-implicit model agrees very well with hydraulic jump theory, while the semi-Lagrangian, explicit model xhibits excessive smoothing and the finite difference model breaks down when the nonlinear interactions become too large. n the second experiment, the system is allowed to rotate to examine the effect of rotation on the formation of topographically nduced hydraulic jumps. Although further study is necessary, it is clear that rotation retards the development of the low ressure to the lee of the obstacle. A larger domain and higher spatial resolution are needed for more detailed simulation of ydraulic jumps.

) Distribution Availability of Abstract] unclassified unlimited ☐ same as report ☐ DTIC users	21 Abstract Security Classification Unclassified	
2a Name of Responsible Individual .oger T. Williams	22b Telephone *(include Area code)* (408) 646-2296	22c Office Symbol 63wu

D FORM 1473,84 MAR 83 APR edition may be used until exhausted
All other editions are obsolete

security classification of this page

Unclassified

Approved for public release; distribution is unlimited.

Semi-Lagrangian, Semi-Implicit Solutions
of the Shallow Water Equations in One Dimension

by

Kristina B. Monk
Second Lieutenant, United States Air Force
B.E.S., Johns Hopkins University, 1985

Submitted in partial fulfillment of the
requirements for the degree of

MASTER OF SCIENCE IN METEOROLOGY

from the

NAVAL POSTGRADUATE SCHOOL
June 1989

Gordon E. Schacher,
Dean of Science and Engineering

ABSTRACT

The semi-Lagrangian, semi-implicit method is used to model the one dimensional shallow water system of equations with surface topography. The forecasts are compared to finite difference and semi-Lagrangian, explicit forecasts. In the first experiment, a non-rotating system is considered. The semi-Lagrangian, semi-implicit model agrees very well with hydraulic jump theory, while the semi-Lagrangian, explicit model exhibits excessive smoothing and the finite difference model breaks down when the nonlinear interactions become too large. In the second experiment, the system is allowed to rotate to examine the effect of rotation on the formation of topographically induced hydraulic jumps. Although further study is necessary, it is clear that rotation retards the development of the low pressure to the lee of the obstacle. A larger domain and higher spatial resolution are needed for more detailed simulation of hydraulic jumps.

TABLE OF CONTENTS

LIST OF TABLES

LIST OF FIGURES

I. INTRODUCTION

There are many numerical methods available for atmospheric modelling, but two features of the semi-Lagrangian, semi-implicit (SLSI) method seem to indicate that it is particularly well suited for numerical weather prediction.

The first of these traits is efficiency. Because the semi-Lagrangian method approximates the total time derivative and the terms responsible for the high frequency gravity waves are treated implicitly, the time step is not limited b_ the Courant-Friedrichs-Lewy stability criterion. Thus, a relatively large time step can be used with the SLSI scheme to produce a timely forecast.

Secondly, a recent investigation by Kuo and Williams (1989) has shown that while more traditional forecast models behave poorly when large gradients develop in a relatively narrow zone, the semi-Lagrangian technique can still produce relatively accurate solutions when a scale-collapse occurs. This is an important attribute for many meteorological applications, such as predicting the formation of squall lines and fronts, or investigating mountain effects.

In this study, the SLSI method is used to model the shallow water system of equations with topography in order to evaluate the handling of mountain effects by the SLSI method. One set of experiments is conducted for the non-rotating system. Several sets of initial conditions are used, some of which are predicted to produce hydraulic jumps. The SLSI forecasts are compared with the forecasts of two other models: a leapfrog finite difference scheme (FDEX), and a semi-Lagrangian, explicit (SLEX) model. Next, the experiments are repeated for a rotating system to examine the effects of rotation on the formation of orographically produced jumps. It is known that rotation can prevent the development of hydraulic jumps in a flat bottom system (Williams and Hori, 1970).

In the next chapter, the development of the semi-Lagrangian technique is reviewed, along with theory on the formation of hydraulic jumps. In Chapter III, the governing equations and formulation of the FDEX, SLEX, and SLSI models are discussed. The initial conditions and results of the experiments are presented in Chapter IV, and conclusions and recommendation for further study are in Chapter V.

II. BACKGROUND

A. THE SEMI-LAGRANGIAN SCHEME

In a pure Lagrangian scheme, such as Fjørtoft (1952) proposed, one set of fluid elements is tracked for the entire integration period. Thus, a parameter, Q, that is conserved following the fluid such that

$$\frac{\partial Q}{\partial t} + V_s \frac{\partial Q}{\partial s} = 0, \qquad (2-1)$$

where s is the direction of the flow and V is the velocity, remains constant with integration. With the more common Eulerian methods, a different set of fluid elements is evaluated at each time step, representing a different distribution of the advective parameters. Fjørtoft's goal was to develop a scheme in which a large time increment, Δt, could be used. In regions of strong wind shear or after long integration periods, however, the initial grid can become greatly distorted, as illustrated in Fig. 1. Data points may cluster in a relatively small area, leaving large areas unanalyzed.

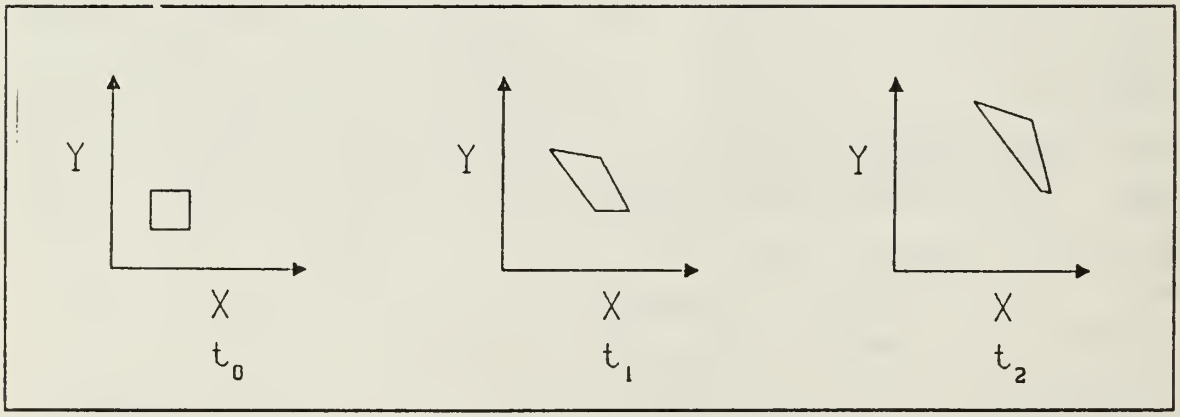

Figure 1. Distortion of Originally Square Grid with Time

To avoid the problem of distortion and still make explicit use of equation (2-1), Wiin-Nielsen (1959) proposed a quasi-Lagrangian, or trajectory, scheme. The fluid's properties are evaluated on a regular, stationary grid at each time step by determining the off-grid positions from which the fluid elements originated.

The semi-Lagrangian method, first proposed by Sawyer (1963), is a modified version of the Wiin-Nielsen scheme. In this study, a one-dimensional, three time level version

of the semi-Lagrangian method, similar to the two-dimensional scheme described by Robert (1981), is used. For each parameter, Q, such that

$$\frac{\partial Q}{\partial t} + U\frac{\partial Q}{\partial x} = R, \qquad (2-2)$$

where R represents all the remaining terms, the left hand side is approximated at the grid point, x_i , by

$$\frac{Q(x_i,t+\Delta t) \quad Q(x_i-2a_i,t-\Delta t)}{2\Delta t} = R, \qquad (2-3)$$

where, by the midpoint rule,

$$a_i = \Delta t \cdot U(x_i - a_i, t). \qquad (2-4)$$

The a_i's must be solved for iteratively. For each n,

$$a_i^n = \Delta t \cdot U(x_i - a_i^{n-1}, t). \qquad (2-5)$$

Subtracting equation (2-4) from (2-5) and applying the Lipschitz condition leads to

$$\frac{\|a_i^n - a_i\|}{\|a_i^{n-1} - a_i\|} = \Delta t \cdot \| \frac{\partial U}{\partial x} \|. \qquad (2-6)$$

Thus, equation (2-5) will converge whenever the right hand side of Equation (2-6) is less than one. Kuo and Williams (1989) argue that no more than three iterations are needed, if this condition is met, since equation (2-4) is only third order accurate with respect to Δt and equation (2-5) becomes order Δt more accurate with each iteration. Pudykiewicz and Staniforth (1984) point out that the maximum horizontal wind shear in most meteorological models is of the order $10^{-4}s^{-1}$, so a time step of $\Delta t \lesssim 3$ hours is necessary for convergence. By contrast, the time step in most Eulerian models used in meteorological applications is restricted by the Courant-Friedrichs-Lewy (CFL) stability criterion,

$$C = U\frac{\Delta t}{\Delta x} < 1, \qquad (2-7)$$

where C is the Courant number. The time step is limited by both the maximum wind speed, U_{max}, and the resolution of the model. For a given U_{max}, the higher the resolution, the smaller the time step.

B. DEVELOPMENT OF HYDRAULIC JUMPS

In this study, the one-dimensional shallow water system of equations is used to examine the nature of the flow of an incompressible, hydrostatic, homogeneous, inviscid fluid over an obstacle in both a non-rotating and rotating system. Under certain conditions, it is possible hydraulic jumps may form in one or both cases.

1. The Non-Rotating System

Houghton and Kasahara (1968) studied the non-rotating shallow water system, illustrated in Fig. 2, and determined the conditions which would lead to the formation of hydraulic jumps. When there is no Coriolis force, i.e. $f = 0$, then the one-dimensional shallow water equations are

$$\frac{\partial u}{\partial t} + u\frac{\partial u}{\partial x} + g\frac{\partial h'}{\partial x} = 0 \qquad (2-8)$$

and

$$\frac{\partial H}{\partial t} + u\frac{\partial H}{\partial x} + H\frac{\partial u}{\partial x} = 0, \qquad (2-9)$$

where u is the horizontal velocity, H is the depth of the fluid and

$$h' = H - h_B. \qquad (2-10)$$

$\frac{\partial h'}{\partial x}$ represents the height perturbation on the free surface.

At $t < 0$, the fluid is at rest, and the free surface is flat. At $t = 0$, the fluid is given a constant velocity of u_o throughout the entire domain. At $t = \infty$, the fluid is at its new steady state given by

$$\frac{u_{ss}^2}{2} + g(H_{ss} + h_B) = \frac{u_o^2}{2} + g\bar{h} = C_1 \qquad (2-11)$$

and

$$u_{ss}H_{ss} = u_o\bar{h} = C_2. \qquad (2-12)$$

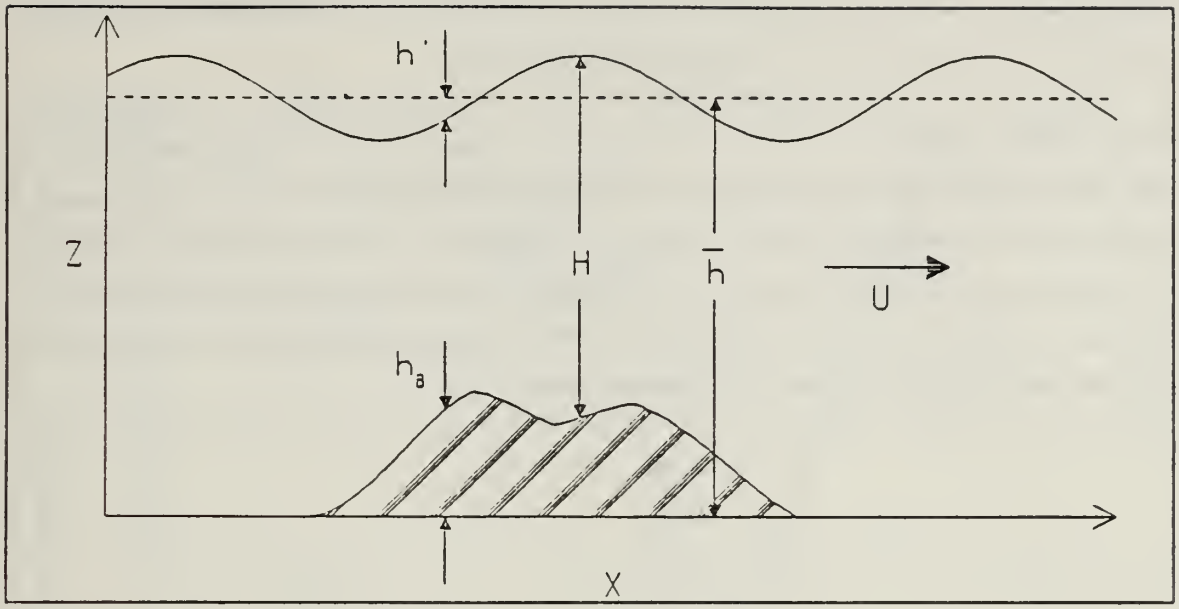

Figure 2. The Shallow Water Model

Eliminating H_{ss} from equation (2-11) using Equation (2-12) and introducing the following dimensionless parameters,

$$Fr = \frac{u_o}{\sqrt{g\bar{h}}}, \quad R = \frac{h_B}{\bar{h}} \quad \text{and} \quad U_* = \frac{u}{u_o}, \tag{2-13}$$

into the resulting equation leads to

$$\frac{Fr^2}{2} U_*^3 + U_*(R - \frac{Fr^2}{2} - 1) + 1 = 0. \tag{2-14}$$

For a given Froude number, Fr, R can be plotted as a function of U_* using equation (2-14). A plot of F versus U_*, shown in Fig. 3 for $Fr^2 = 0.1$, illustrates there are three real roots to equation (2-14) if $R < R_{CRITICAL}$. Only one of these roots is physically meaningful. If $R > R_{CRITICAL}$, only one solution to equation (2-14) exists, but since this solution has no physical meaning, a hydraulic jump is anticipated. $R_{CRITICAL}$ can be expressed as a function of the Froude number:

$$R_{CRITICAL} = \frac{1}{2} Fr^2 - \frac{3}{2} Fr^{\frac{2}{3}} + 1. \tag{2-15}$$

A plot of $R_{CRITICAL}$ versus Fr, illustrated in Fig. 4 indicates the three classes of solution to equation (2-14) identified by Houghton and Kasahara.

Domain I is the subcritical range in which $R < R_{CRITICAL}$ and $Fr < 1$. The steady state free surface height of a fluid flow which meets these criteria will dip over the obstacle. The velocity will increase over the obstacle but will remain less than u_*, the speed that corresponds to the condition $R = R_{CRITICAL}$. Domain II is the 'jump region' in which $R > R_{CRITICAL}$ and a hydraulic jump forms. Domain III is the supercritical range in which $R < R_{CRITICAL}$, but $Fr > 1$. At its steady state, the free surface height rises over the obstacle, and the velocity decreases but remains greater than u_*.

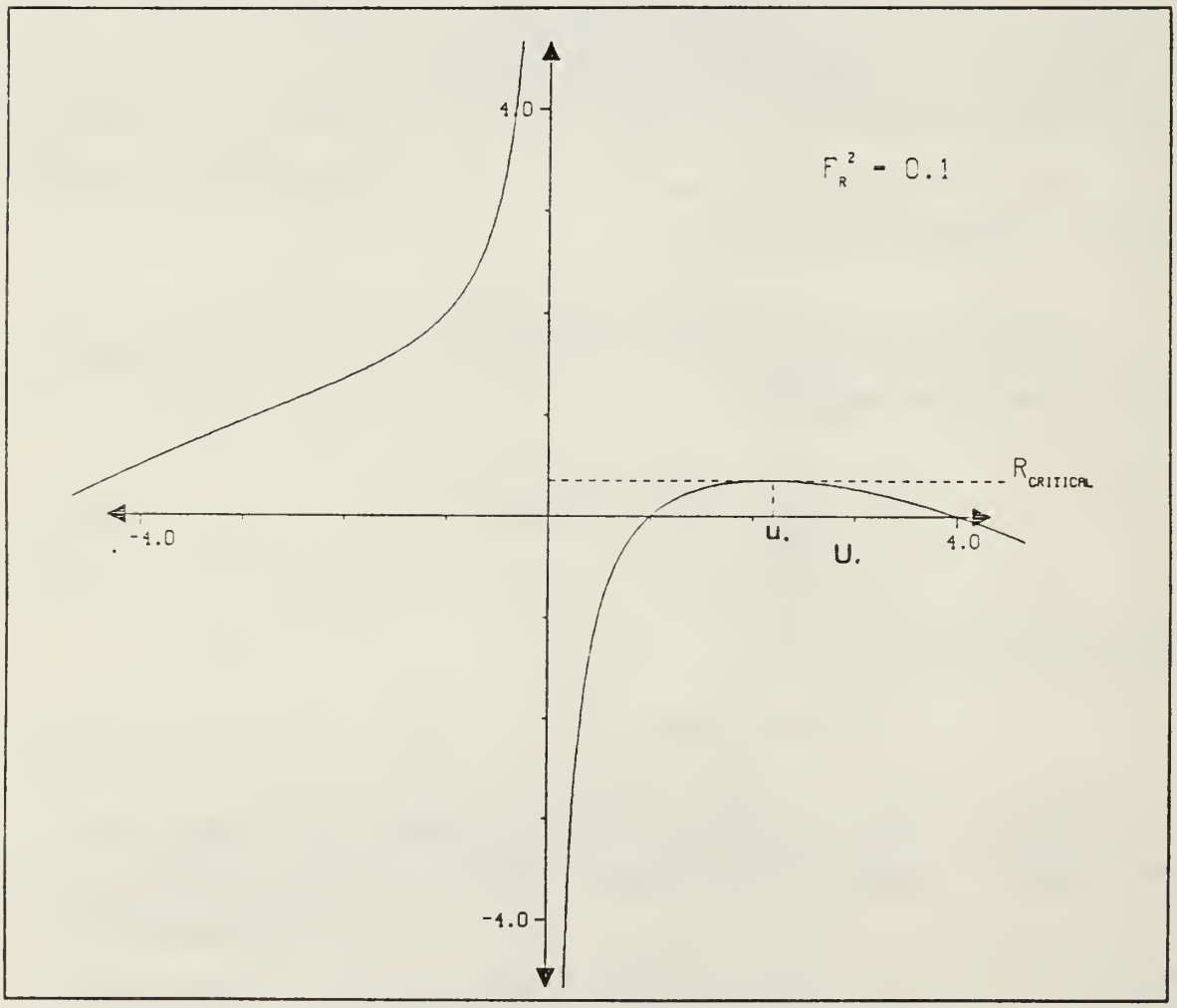

Figure 3. $R_{CRITICAL}$ versus U_* for $Fr^2 = 0.1$

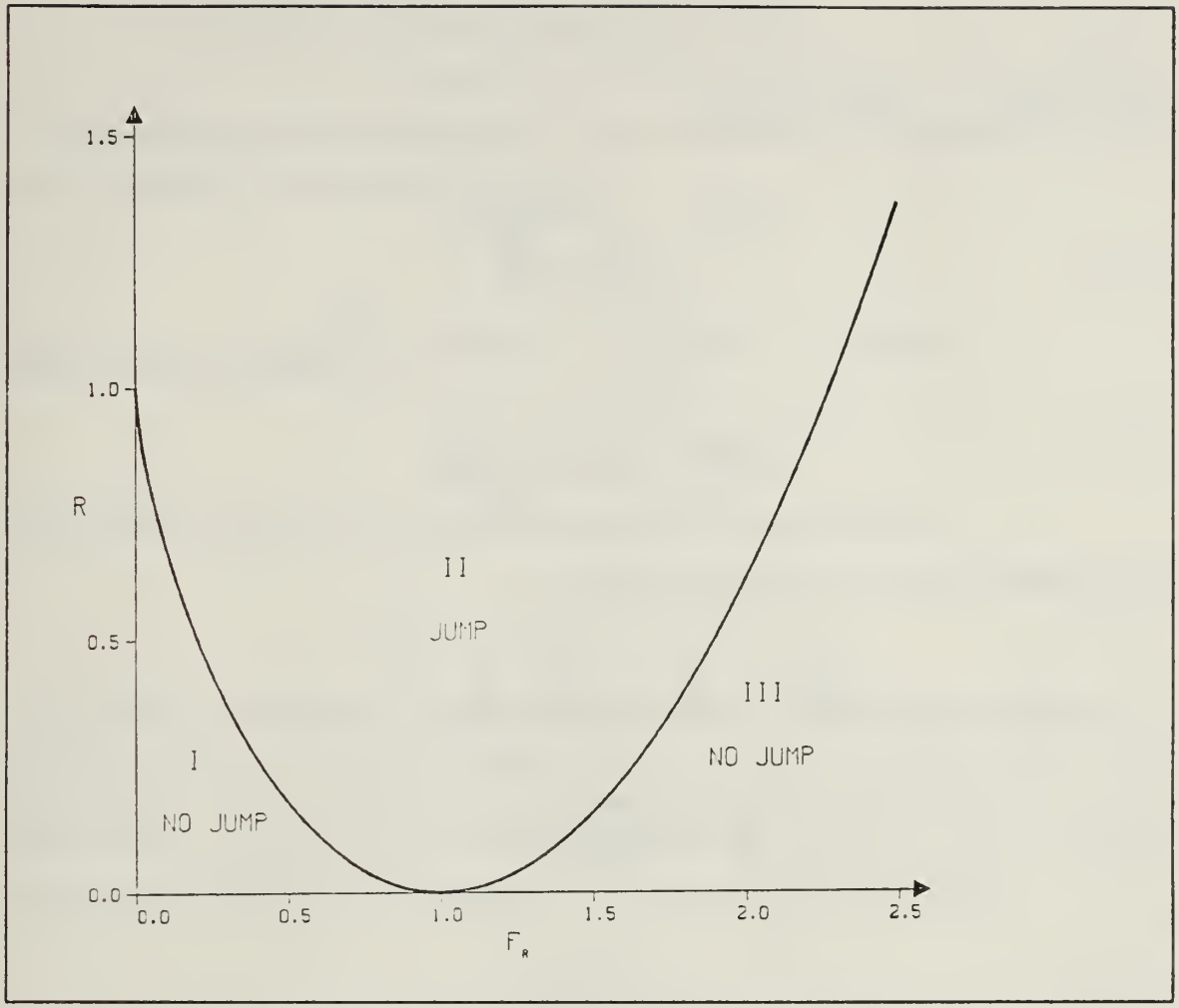

Figure 4. $R_{CRITICAL}$ versus Fr

2. The Effect of Rotation

If the coordinate system is rotating, i.e. $f \neq 0$, then the shallow water system equations for a flat lower boundary and no y dependence are

$$\frac{\partial u}{\partial t} + u\frac{\partial u}{\partial x} + g\frac{\partial H}{\partial x} - fv = 0, \qquad (2-16)$$

$$\frac{\partial v}{\partial t} + u\frac{\partial v}{\partial x} + fu = 0 \qquad (2-17)$$

and

$$\frac{\partial H}{\partial t} + u\frac{\partial H}{\partial x} + H\frac{\partial u}{\partial x} = 0. \qquad (2-18)$$

If the variables are scaled as follows:

$$x = Lx_s, \qquad t = \frac{L}{\sqrt{gh_m}}t_s,$$

$$u = Uu_s, \qquad v = \left(\frac{Fr}{R_o}\right)v_s, \qquad H = \bar{h} + U\sqrt{\frac{\bar{h}}{g}}h_s, \qquad (2-19)$$

$$R_o = \frac{U}{fL} \quad \text{and} \quad F = \frac{U}{\sqrt{g\bar{h}}},$$

then equations (2-16), (2-17) and (2-18) become

$$\frac{\partial u_s}{\partial t_s} + Fu_s\frac{\partial u_s}{\partial x_s} + g\frac{\partial h_s}{\partial x_s} - \frac{F^2}{R_o^2}v = 0, \qquad (2-20)$$

$$\frac{\partial v_s}{\partial t_s} + Fu_s\frac{\partial v_s}{\partial x_s} + u_s = 0 \qquad (2-21)$$

and

$$\frac{\partial h_s}{\partial t_s} + F\left(u_s\frac{\partial h_s}{\partial x_s} + h_s\frac{\partial u_s}{\partial x_s}\right) + \frac{\partial u_s}{\partial x_s} = 0. \qquad (2-22)$$

Unless the Coriolis term dominates, hydraulic jumps may form due to the nonlinear advection terms. The no-jump condition can be expressed as

$$\frac{F^2}{R_o^2} \gg F, \qquad (2-23)$$

or

$$F = A \cdot R_o^2, \qquad (2-24)$$

where A is some number much larger than one. The Williams and Hori (1970) investigation found that A is in the range of 6.5 to 7.0.

3. Scale Collapse Problem

Computational difficulties may arise when a numerical model must represent a physical process in which a large gradient or discontinuity forms. Kuo and Williams (1989) considered a simple scale-collapse case, for which the governing equation was the one dimensional nonlinear advection equation

$$\frac{\partial u}{\partial t} + u\frac{\partial u}{\partial x} = 0, \qquad (2-25)$$

and the initial condition

$$u(x)_{t=0} = -\tan^{-1}(x - x_o). \qquad (2-26)$$

This problem can be solved for analytically, and that solution leads to

$$\frac{\partial u}{\partial x}\Big|_{x=x_o} = \frac{1}{t-1} \to -\infty \ \ as \ \ t \to 1_-. \qquad (2-27)$$

Kuo and Williams compared the second-order centered finite difference, the Chebyshev-Tau and the semi-Lagrangian solutions of equation (2-25) and (2-26). The scale-collapse at $x = x_o$ produces large, fluctuating errors throughout the entire domain when either the finite difference or Chebyshev-Tau method is used. The semi-Lagrangian method responds differently. As t approaches one from below,

$$\Delta t \cdot \| \frac{\partial U}{\partial x} \| > 1, \qquad (2-28)$$

for $i\Delta x \approx x_o$. Therefore, equation (2-5) will not converge in this region. However, if a fixed number of iterations ($n = 3$) is used to solve for the a_i's, the errors which result when and where equation (2-28) is true remain near the scale collapse zone. Thus, the semi-Lagrangian method is still useful even after discontinuities develop.

In this study, two semi-Lagrangian schemes for the shallow water equations are compared with the traditional leap-frog finite difference method. In the first, the R terms in equation (2-2) are treated explicitly; that is, they are evaluated at $(x_i - a_i, t)$. This scheme is expected to handle large shear zones, but the freedom from the CFL criterion cannot be exploited, because the time step is still limited by the gravity wave terms. The second scheme is a semi-Lagrangian, semi-implicit scheme similar to the one presented by Pudykiewicz and Staniforth (1984), but modified to include topographical effects. The terms responsible for the gravity waves are treated implicitly by averaging between

$(x_i, t + \Delta t)$ and $(x_i - 2a_i, t - \Delta t)$. The remaining terms are evaluated at $(x_i - a_i, t)$. The semi-Lagrangian, semi-implicit scheme requires more computational effort, but it permits a much greater time step.

III. FORMULATION OF THE MODELS

A. THE GOVERNING EQUATIONS

The governing equations for the shallow water model, illustrated in Fig. 2, are

$$\frac{\partial u}{\partial t} + u\frac{\partial u}{\partial x} + g\left(\frac{\partial H}{\partial x} + \frac{\partial h_B}{\partial x}\right) - fv = 0, \tag{3-1}$$

$$\frac{\partial v}{\partial t} + u\frac{\partial v}{\partial x} + g\left(\frac{\partial H}{\partial y} + \frac{\partial h_B}{\partial y}\right) + fu = 0 \tag{3-2}$$

and

$$\frac{\partial H}{\partial t} + \frac{\partial}{\partial x}(uH) + \frac{\partial}{\partial y}(vH) = 0. \tag{3-3}$$

In the one-dimensional model, the mean flow, V_o, is zonal and in geostrophic balance with the mean free surface height, such that

$$u_o = -\frac{g}{f}\frac{\partial \bar{h}}{\partial y} \tag{3-4}$$

and

$$v_o = \frac{g}{f}\frac{\partial \bar{h}}{\partial x} = 0, \tag{3-5}$$

and perturbations in the dependent variables, u', v' and h' are in the x direction only. Multiplying equation (3-3) by g and substituting

$$u(x,t) = u_o + u'(x,t), \tag{3-6}$$

$$v(x,t) = v'(x,t) \tag{3-7}$$

and

$$\phi(x,t) = \bar{\phi}(y) - \phi_B(x,y) + \phi'(x,t) = gH \tag{3-8}$$

into equations (3-1), (3-2) and (3-3) yields the following set of equations

$$\frac{\partial u'}{\partial t} + (u_o + u')\frac{\partial u'}{\partial x} + \frac{\partial \phi'}{\partial x} - fv' = 0, \qquad (3-9)$$

$$\frac{\partial v'}{\partial t} + (u_o + u')\frac{\partial v'}{\partial x} + fu' = 0 \qquad (3-10)$$

and

$$\frac{\partial \phi'}{\partial t} + (u_o + u')\left(\frac{\partial \phi'}{\partial x} - \frac{\partial \phi_B}{\partial x}\right) + (\bar{\phi} - \phi_B + \phi')\left(\frac{\partial u'}{\partial x}\right) +$$

$$v'\left(\frac{\partial \bar{\phi}}{\partial y} - \frac{\partial \phi_B}{\partial y}\right) = 0. \qquad (3-11)$$

For convenience, the bottom topography is assumed to be parallel to the mean free surface height in the y direction, so that

$$\frac{\partial \bar{h}}{\partial y} = \frac{\partial h_B}{\partial y} \qquad (3-12)$$

and equation (3-11) reduces to

$$\frac{\partial \phi'}{\partial t} + (u_o + u')\left(\frac{\partial \phi'}{\partial x} - \frac{\partial \phi_B}{\partial x}\right) + (\bar{\phi} - \phi_B + \phi')\frac{\partial u'}{\partial x} = 0. \qquad (3-13)$$

B. FINITE DIFFERENCE SCHEME

One of the simplest numerical methods is finite differencing centered in time and space, the leapfrog scheme. On the staggered grid, equations (3-9), (3-10) and (3-13) approximated by this method become

$$\frac{u'(x,t+\Delta t) - u'(x,t-\Delta t)}{2t} + (u_o + u'(x,t))\left[\frac{u'(x+\Delta x,t) - u'(x-\Delta x,t)}{2\Delta x}\right] =$$

$$-\frac{\phi'(x+\frac{\Delta x}{2},t) - \phi'(x-\frac{\Delta x}{2},t)}{\Delta x} + f\left[\frac{v'(x-\frac{\Delta x}{2},t) + v'(x+\frac{\Delta x}{2},t)}{2}\right], \qquad (3-14)$$

$$\frac{v'(x,t+\Delta t) - v'(x,t-\Delta t)}{2\Delta t} + \bar{u}(x,t)\left[\frac{v'(x+\Delta x,t) - v'(x-\Delta x,t)}{2\Delta x}\right] =$$

$$-f\left[\frac{u'(x+\frac{\Delta x}{2},t)+u'(x-\frac{\Delta x}{2},t)}{2}\right] \qquad (3-15)$$

and

$$\frac{\phi'(x,t+\Delta t)-\phi'(x,t-\Delta t)}{2\Delta t}+\bar{u}(x,t)\left[\frac{\phi'(x+\Delta x,t)-\phi'(x-\Delta x,t)}{2\Delta x}\right]=$$

$$\bar{u}(x,t)\left[\frac{\phi_B(x+\Delta x)-\phi_B(x-\Delta x)}{2\Delta x}\right]$$

$$-(\bar{\phi}-\phi_B(x)+\phi'(x,t))\left[\frac{u'(x+\frac{\Delta x}{2},t)-u'(x-\frac{\Delta x}{2},t)}{\Delta x}\right]. \qquad (3-16)$$

where

$$\bar{u}(x,t)=u_\circ+\left[\frac{u'(x-\frac{\Delta x}{2},t)+u'(x+\frac{\Delta x}{2},t)}{2}\right]. \qquad (3-17)$$

C. SEMI-LAGRANGIAN, EXPLICIT SCHEME

The second numerical scheme uses the semi-Lagrangian method described by Robert (1981), modified for one dimensional flow over a surface with topography. The remaining terms are centered in space about $(x-a,t)$. Equations (3-9), (3-10) and (3-13) approximated by this method become

$$\frac{u'(x,t+\Delta t)-u'(x-2a,t-\Delta t)}{2\Delta t}=-\frac{\delta\phi'}{\delta x}\Big|_{(x-a,t)}+fv'(x-a,t), \qquad (3-18)$$

$$\frac{v'(x,t+\Delta t)-v'(x-2a,t-\Delta t)}{2\Delta t}=-fu'(x-a,t) \qquad (3-19)$$

and

$$\frac{\phi'(x,t+\Delta t)-\phi'(x-2a,t-\Delta t)}{2\Delta t}-\frac{\phi_B(x)-\phi_B(x-2a)}{2\Delta t}=$$

$$- \left((\bar{\phi} - \phi_B + \phi') \frac{\delta u'}{\delta x} |_{(x-a,t)} \right), \qquad (3-20)$$

where

$$\frac{\partial Q}{\partial x} |_{(x)} \approx \frac{\delta Q}{\delta x} |_{(x)} = \frac{Q(x + \frac{\Delta x}{2}) - Q(x - \frac{\Delta x}{2})}{\Delta x}. \qquad (3-21)$$

Equation (3-21) is used to estimate $\frac{\partial \phi'}{\partial x}$ and $\frac{\partial u'}{\partial x}$ at the grid points, and then an interpolation scheme is used to evaluate these terms at $(x-a)$. An alternative method would be to approximate the derivatives immediately at $(x-a)$ with the following equation:

$$\frac{\delta Q}{\delta x} |_{(x-a)} = \frac{Q(x - a + \frac{\Delta x}{2}) - Q(x - a - \frac{\Delta x}{2})}{\Delta x}. \qquad (3-22)$$

Although this method appears more direct than using equation (3-21), it requires twice as many interpolations and therefore more computational effort.

Note,

$$\bar{u} \frac{\partial \phi_B}{\partial x} = \frac{\partial \phi_B}{\partial t} + \bar{u} \frac{\partial \phi_B}{\partial x} \approx \frac{\phi_B(x) - \phi_B(x - 2a)}{2\Delta t}, \qquad (3-23)$$

since there is no local time change in the bottom topography, i.e., $\frac{\partial \phi_B}{\partial t}$ is zero.

D. SEMI-LAGRANGIAN, SEMI-IMPLICIT SCHEME

This scheme is similar to the semi-Lagrangian, explicit scheme presented above except the gravity wave terms are treated semi-implicitly. The development of this scheme is similar to the development of the semi-Lagrangian, semi-implicit scheme developed by Staniforth and Temperton (1986) for a flat bottom system. The finite difference equations now become

$$\frac{u'(x,t+\Delta t) - u'(x-2a,t-\Delta t)}{2\Delta t} = -\frac{1}{2}\left[\frac{\delta \phi'}{\delta x} |_{(x,t+\Delta t)} + \frac{\delta \phi'}{\delta x} |_{(x-2a,t-\Delta t)} \right]$$

$$+ fv'(x-a,t), \qquad (3-24)$$

$$\frac{v'(x,t+\Delta t) - v'(x-2a,t-\Delta t)}{2\Delta x} = -fu'(x-a,t) \qquad (3-25)$$

and

$$\frac{\phi'(x,t+\Delta t)-\phi'(x-2a,t-\Delta t)}{2\Delta t}-\frac{\phi_B(x)-\phi_B(x-2a)}{2\Delta t}=-\phi\frac{\delta u'}{\delta x}\Big|_{(x-a,t)}$$

$$-\frac{1}{2}\left[(\overline{\phi}-\phi_B(x))\frac{\delta u'}{\delta x}\Big|_{(x,t+\Delta t)}+(\overline{\phi}-\phi_B(x-2a))\frac{\delta u'}{\delta x}\Big|_{(x-2a,t-\Delta t)}\right]. \quad (3-26)$$

The divergence term at $(t+\Delta t)$ is eliminated from equation (3-26) by first finite differentiating equation (3-24) with respect to x, which yields,

$$\frac{\delta u'}{\delta x}\Big|_{(x,t+\Delta t)}=\frac{\delta u'}{\delta x}\Big|_{(x-2a,t-\Delta t)}-\Delta t\left[\frac{\delta^2\phi'}{\delta x^2}\Big|_{(x,t+\Delta t)}+\frac{\delta^2\phi'}{\delta x^2}\Big|_{(x-2a,t-\Delta t)}\right]$$

$$+2\Delta t f\frac{\delta v}{\delta x}\Big|_{(x-a,t)}, \quad (3-27)$$

where

$$\frac{\delta^2\phi'}{\delta x^2}=\frac{\phi'(x+\Delta x)-2\phi'(x)+\phi'(x-\Delta x)}{\Delta x^2}, \quad (3-28)$$

then substituting equation (3-27) into (3-26) and collecting all $(x,t+\Delta t)$ terms on the left-hand side

$$\left(\frac{\delta^2}{\delta x^2}-\frac{1}{\Delta t^2(\overline{\phi}-\phi_B(x))}\right)\phi'(x,t+\Delta t)=-\left(\frac{\delta^2}{\delta x^2}+\frac{1}{\Delta t^2(\overline{\phi}-\phi_B(x))}\right)\phi'(x-2a,t-\Delta t)$$

$$-\frac{\phi_B(x)-\phi_B(x-2a)}{\Delta t^2(\overline{\phi}-\phi_B(x))}+\left(\frac{1}{\Delta t}+\frac{\overline{\phi}-\phi_B(x-2a)}{\overline{\phi}-\phi_B(x)}\right)\frac{\delta u'}{\delta t}\Big|_{(x-2a,t-\Delta t)}$$

$$+\frac{2\phi'(x-a)}{\Delta t(\overline{\phi}-\phi_B(x))}\frac{\delta u'}{\delta x}\Big|_{(x-a,t)}+2f\frac{\delta v'}{\delta x}\Big|_{(x-a,t)}, \quad (3-29)$$

or, expanding,

$$\frac{\phi'(x+\Delta x)-\left(2+\dfrac{\Delta x^2}{\Delta t^2(\overline{\phi}-\phi_B(x))}\right)\phi'(x)+\phi'(x-\Delta x)}{\Delta x^2}\Big|_{t+\Delta t}=$$

$$-\frac{\phi'(x-2a+\Delta x)-\left(2-\frac{\Delta x^2}{\Delta t^2(\overline{\phi}-\phi_B(x-2a))}\right)\phi'(x-2a)+\phi'(x-2a-\Delta x)}{\Delta x^2}\Big|_{t-\Delta t}$$

$$-\frac{\phi_B(x)-\phi_B(x-2a)}{\Delta t^2(\overline{\phi}-\phi_B(x))}+\left(\frac{1}{\Delta t}+\frac{\overline{\phi}-\phi_B(x-2a)}{\Delta t(\overline{\phi}-\phi_B(x))}\right)\left[\frac{u'(x-2a+\frac{\Delta x}{2})-u'(x-2a-\frac{\Delta x}{2})}{\Delta x}\right]\Big|_{t-}$$

$$+\frac{2\phi'(x-a)}{\Delta t(\overline{\phi}-\phi_B(x))}\left[\frac{u'(x-a+\frac{\Delta x}{2})-u'(x-a-\frac{\Delta x}{2})}{\Delta x}\right]\Big|_t$$

$$+f\left[\frac{v'(x+a+\Delta x)-v'(x-a-\Delta x)}{\Delta x}\right]\Big|_t \qquad (3-30)$$

Equation (3-30) can be written in matrix form as

$$[A]\{\phi'_i\}=\{B_i\}, \qquad (3-31)$$

where $\{B_i\}$ are all the terms on the right-hand side of equation (3-28) and the matrix A is

$$[A]=\begin{bmatrix} \alpha_1 & 1 & 0\ldots & & \ldots 0 & 1 \\ 1 & \alpha_2 & 1 & 0\ldots & & \ldots 0 \\ & & & & & \\ 0\ldots & & \ldots 0 & 1 & \alpha_{N-1} & 1 \\ 1 & 0\ldots & & \ldots 0 & 1 & \alpha_N \end{bmatrix}, \qquad (3-32)$$

where

$$\alpha_i=-\left(2+\frac{\Delta x^2}{\Delta t^2(\overline{\phi}-\phi_B(i\Delta x))}\right). \qquad (3-33)$$

To solve equation (3-31), it is necessary to invert the matrix A :

$$\{\phi'_i\}=[A]^{-1}\{B_i\}. \qquad (3-34)$$

However, since matrix A has no time dependent elements, the inverse, $[A]^{-1}$, must be solved for only once.

E. THE SPATIAL GRID

u', v' and ϕ', are evaluated on the staggered grid, scheme C of Arakawa and Lamb (1977), illustrated in Fig. 5. The use of scheme C further limits the maximum time step for the explicit models, already restricted by the CFL criterion, by a factor of two, as Haltiner and Williams (1980) demonstrated with the leapfrog finite difference scheme. However, they also showed that scheme C simulates the shorter waves far better than the unstaggered grid, an important feature when investigating orographic effects. Cyclic boundary conditions are used to avoid the difficulties associated with the advection of fluid elements from outside the domain onto the grid.

An interpolation scheme is needed to evaluate the dependent variables at $(x - a)$ and $(x - 2a)$, but the resultant smoothing of the variables between grid points can represent significant errors. Kuo and Williams (1989) have shown that in regions where the Courant number is less than one, interpolation errors dominate time truncation errors. In these situations, the forecasts become more accurate as Δt is increased, because fewer time steps require fewer interpolations.

In this study, a cubic spline interpolator is used. Although computationally expensive, the cubic spline, because of it accuracy, has been a popular choice for use with the semi-Lagrangian method (Robert (1981), Pudykiewicz and Staniforth (1984), Ritchie (1987), Kuo and Williams (1989).) The global nature of the cubic spline (all grid values are used to estimate to a single point), led Pudykiewicz and Staniforth (1984) to suggest that this scheme would be inappropriate where locally steep gradients occur and to speculate that a local interpolating function should be used in these situations to minimize the Gibbs' phenomenon. However, Kuo's and Williams' (1989) investigation of a scale collapse model found that the deviations in semi-Lagrangian forecast from the analytical solution remained small and confined to the region of the large wind convergence, even though a cubic spline interpolator was used.

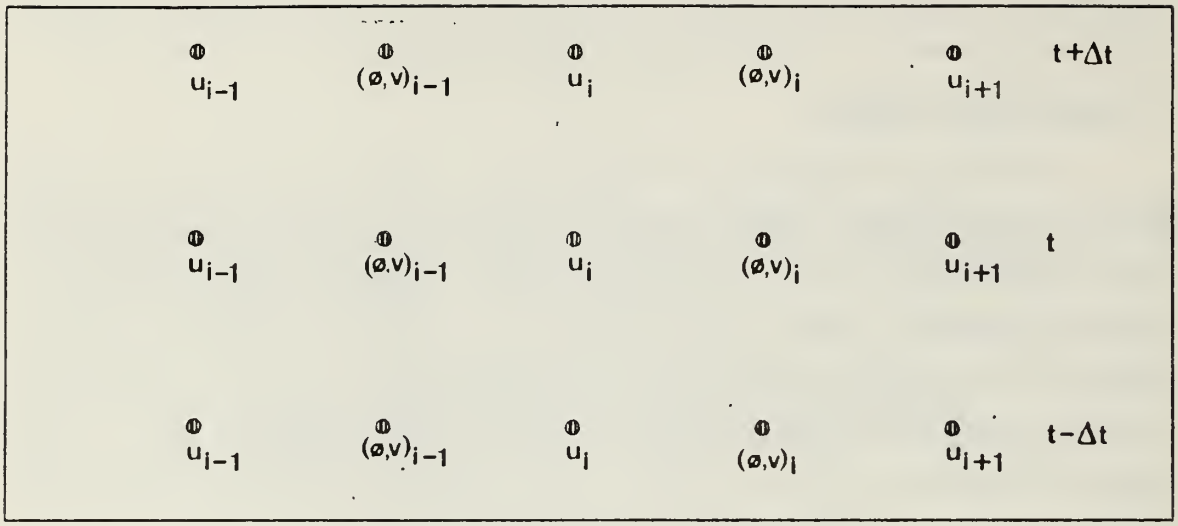

Figure 5. Staggered Grid

IV. EXPERIMENTS AND RESULTS

In the first experiment, the three models' forecasts for flow over a topographical ridge in a non-rotating system are compared. The same cases that Petroliagis (1988) investigated with a Galerkin model are examined here. All three domains identified by Houghton and Kasahara (1968) are represented.

In the second experiment, the effect of rotation upon topographically induced jump formations is examined. The three models are run with the same sets of parameters used in the first experiment, except $f = 0.000103\ \text{sec}^{-1}$, corresponding to the Coriolis force at 45° N.

A. INITIAL CONDITIONS

The domain of integration, L, is 7276 km in the x direction, divided into 48 increments of length $\frac{\Delta x}{2}$. u is evaluated on the odd numbered grid points; v and ϕ are evaluated on the even numbered grid points. The boundary conditions are cyclic, such that

$$u(0) = u(L), \qquad v(0) = v(L) \text{ and } \phi(0) = \phi(L). \tag{5-1}$$

The ridge profile, illustrated in Fig. 6 is described by

$$h_B = \begin{cases} H_B \sin^2\left(\dfrac{\pi(i-20)}{12}\right) & \text{for } 20\Delta x \le x \le 32\Delta x \\ 0 & \text{elsewhere.} \end{cases} \tag{5-2}$$

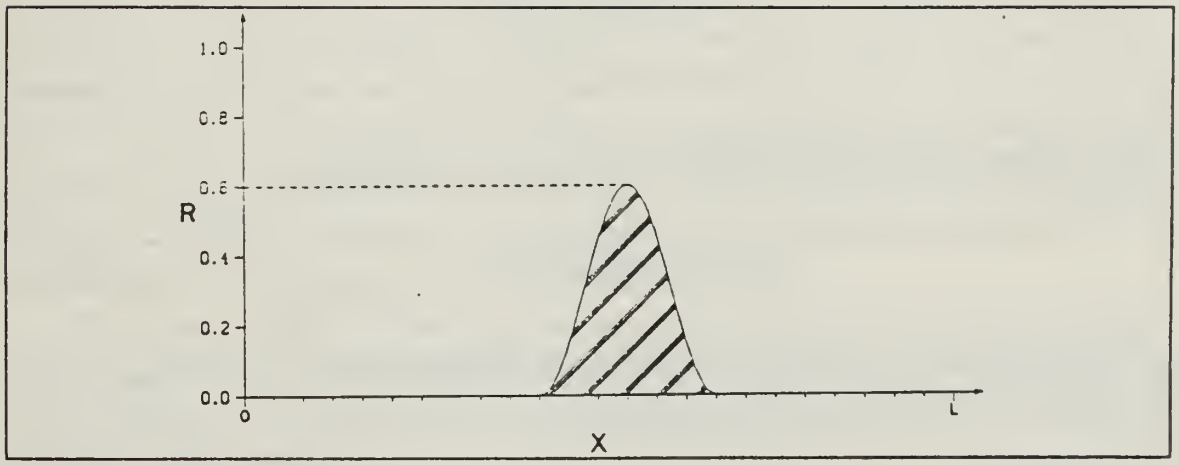

Figure 6. Profile of the North-South ridge

The five cases examined, summarized in Table 1, are parameterized by the mean height, $\bar{h}$, the ratio of the mountain peak to the mean height, R, and the Froude number, Fr. These are the same sets of parameters that Petroliagis (1988) used. However, for these experiments L and Δx are increased tenfold which increases the time scale, so that f could be important in the second set of experiment.

Table 1. PARAMETERS FOR CASES I THROUGH V

CASE	$\bar{h}$ (m)	R	Fr	u_o (m s)	D
I	1000.	0.2	0.1	19.8	I
II	1000.	0.2	0.4	39.6	I
III	1000.	0.7	0.3	29.7	II
IV	500.	0.2	0.8	56.0	II
V	400.	0.05	1.4	87.7	III

A five-minute time step, Δt_{EX}, is used with the Finite Difference Explicit (FDEX) and Semi-Lagrangian Explicit (SLEX) models. A one-hour time step, Δt_{SI}, is used with the Semi-Lagrangian Semi-Implicit (SLSI) model. The Semi-Lagrangian Semi-Implicit model is also run at a higher resolution (HRSL) for comparison with the other models. For HRSL, Δx is reduced by a factor of four, and Δt_{SI} is used.

Δt_{EX} is limited by the CFL stability criterion based on the speed of the explicitly treated external gravity waves. The mean speed of these waves, c, is given by

$$c = | u_o \pm \sqrt{\bar{\phi}} | ,$$

$$= | (Fr \pm 1)\sqrt{\bar{\phi}} | . \qquad (4-3)$$

A mean Courant number for the explicit cases, C_{EX}, can be defined as

$$C_{EX} \equiv \left| 2 \frac{c\Delta t_{EX}}{\Delta x} \right| < 1. \qquad (4-$$

As discussed in chapter 3, the factor of two arises because scheme C is used. C_{EX} is approximately 0.25-0.30 for the cases considered.

B. RESULTS I

The u field for case I after two, four, six and eight hours of integration are shown in Fig. 7. All the models produce a stationary speed maximum centered over the ridge,

which the theory predicts for the subcritical range (Domain I). FDEX and SLEX slightly underdevelop the speed maximum while SLSI is in good agreement with HRSL. All the models show the development of a secondary maximum that propagates eastward. After eight hours the downstream disturbances have propagated around to the east side of the ridge and begin to interfere with the upstream fields.

As anticipated, a low pressure region develops on the lee side of the mountain (Fig. 8). The high pressure field to the east of the ridge remains fairly stationary in the SLSI and HRSL forecasts. This feature drifts upstream perceptibly in the FDEX and SLEX forecasts. Theory predicts the formation of a wave train on the lee side of the mountain. FDEX, SLEX and SLSI all lag behind the high resolution model in developing these waves. SLSI is only slightly behind. The FDEX becomes appreciably damped, but SLEX has the poorest results due to excessive smoothing after numerous interpolations.

Case II is also in Domain I, however the mean flow, U_{MEAN}, is stronger and the mountain peak, H_B, is higher. Although the perturbations are relatively larger, the u and ϕ' fields, shown in Fig. 9 and Fig. 10 for two, four, six and eight hours, are quite similar to their counterparts in case I.

Case III and case IV lie in Domain II, so hydraulic jumps are anticipated. Fig. 11 and Fig. 12 illustrate the u and ϕ' fields at three, six, nine and twelve hours for case III. All models forecast a wind speed maximum over the ridge. The FDEX solution does not appear in Fig. 11C and Fig. 11D and in Fig. 12C and Fig. 12D, because FDEX is unstable, failing to converge after six hours, due to the large nonlinear interactions in the vicinity where the jump is developing. The HRSL model continues to deepen and broaden the pressure minimum on the lee side of the ridge until, after eleven hours of integration, the pressure has dropped to zero. Once the free surface height hits the bottom topography, the integration is stopped. The perturbation fields develop slightly slower in the SLSI model; the free surface hits the bottom after 13 hours of integration. Initially, the SLEX forecasts are very similar to SLSI's. With time, however, the SLEX perturbations dampen out, again due to interpolation error.

The u and ϕ' fields at three, six, nine and twelve hours for case IV are shown in Fig. 13 and Fig. 14. The amplitude of disturbances are increasing, but because of the cyclic boundary conditions, there is interference from the transient part of the solution before a jump can form.

Case V is in Domain III, the supercritical range. The u and ϕ' fields from all the models are compared in Fig. 15 and Fig. 16. SLSI again agrees well with HRSL. Both

produce the speed minimum over the ridge as the theory predicts. FDEX and SLEX develop this minimum slightly upstream. All the models show a pressure minimum to the lee of the obstacle. The SLSI and HRSL remain rather stable, until the transient solutions propagating to the east circle back around to the west of the ridge. The SLEX model exhibits exceesive smoothing from accumulating interpolation errors, as it does for all the other cases. The FDEX solution becomes unstable in this case, unable to handle the nonlinear interactions when Fr exceeds one.

C. RESULTS II

W en the system is allowed to rotate, perturbations arise in v as well as in u and ϕ. These disturbances in v are out of phase with the u' field, as illustrated in Fig. 17 for case I. After several hours of integration, perturbations in u are noticably smaller and the pressure drop on the lee side of the obstacle appears not as deep when compared to the non-rotating cases, as in Fig. 18A and Fig. 18B for the HRSL results for case II. Although the Coriolis force is deflecting some energy into the y direction, cases III and IV are still unstable. For both cases, the amplitudes of the disturbances in the vicinity of the ridge continually increase. This is illustrated in Fig. 19 for the total u field in case IV after three, six, nine and twelve hours of integration.

Fig. 19 is also representative of the relative performance of the models for all cases in the rotating system. Not suprisingly, the results of these comparisons are much the same as in the non-rotating cases. SLSI agrees most closely with the high resolution model. FDEX is unable to capture all the details in the disturbance fields and has a tendency to place the extrema slightly upstream from the HRSL model. The SLEX forecasts are the poorest due to the dominance of interpolation errors.

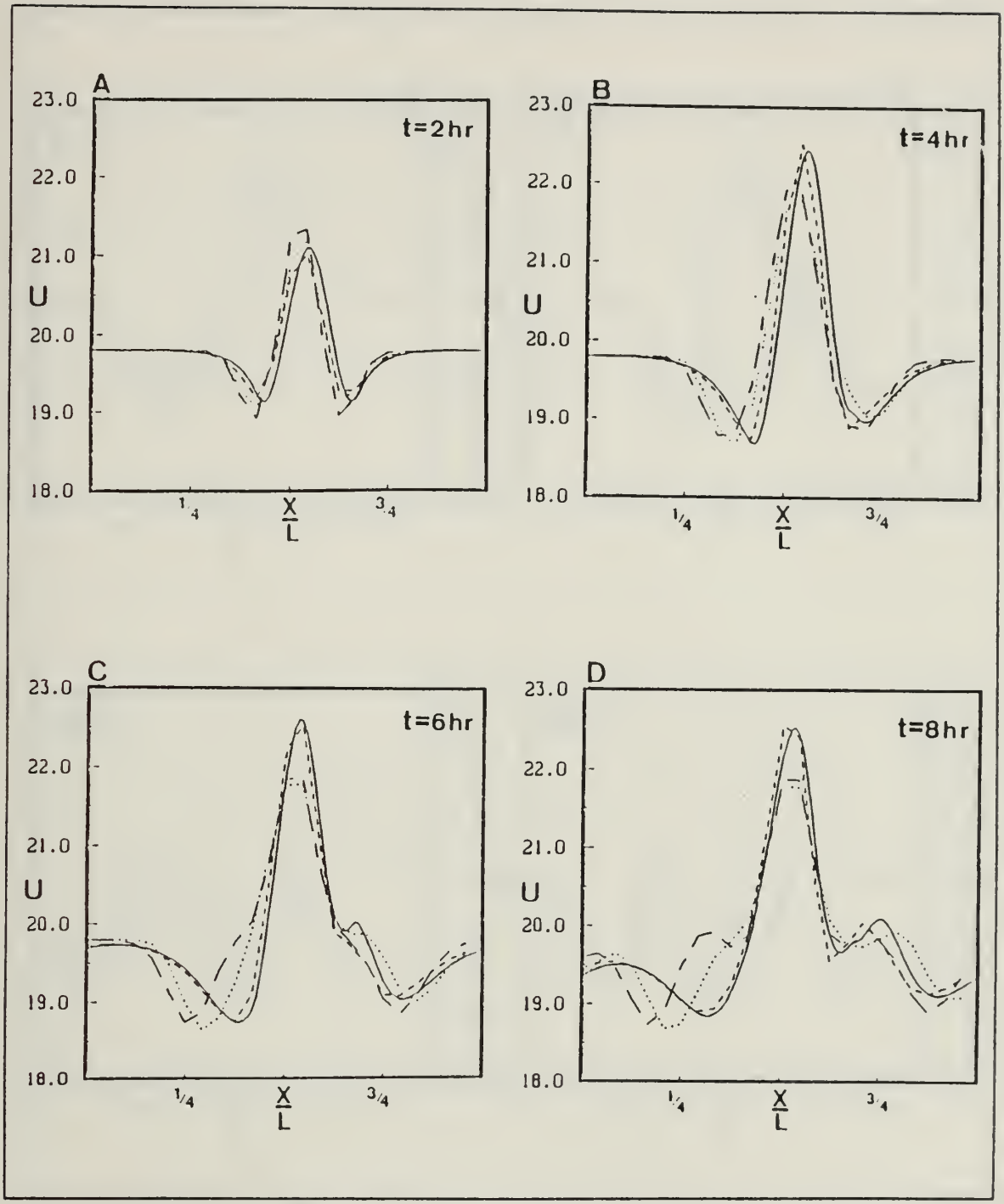

Figure 7. Experiment 1, Case I: Total *u* Field (*m/s*) after A) Two B) Four C) Six D) Eight Hours of Integration for HRSL (solid line), SLSI (dashed line), SLEX (broken line) and FDEX (dotted line).

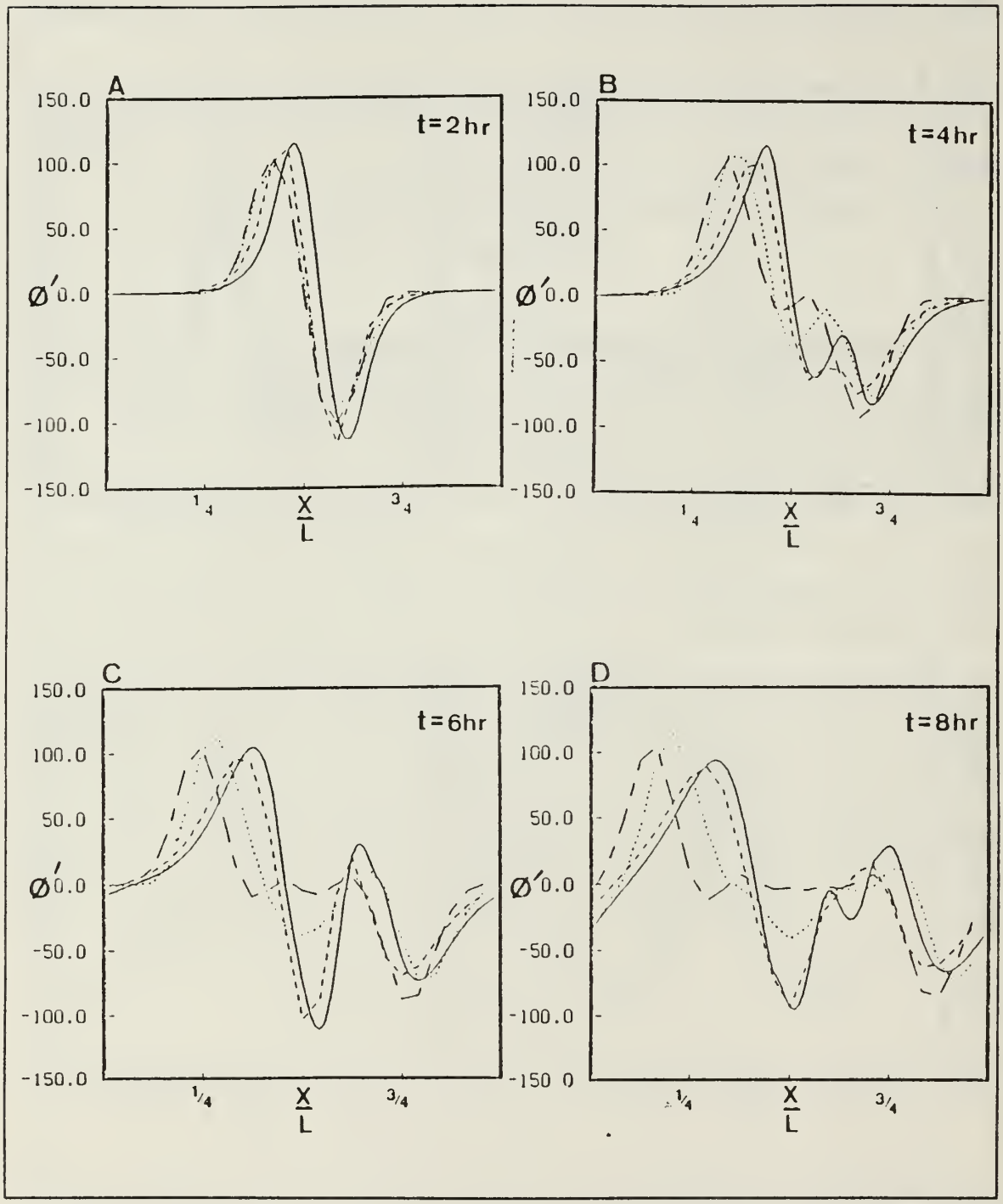

Figure 8. Experiment 1, Case I: ϕ' Field $(m/s)^2$ after A) Two B) Four C) Six D) Eight Hours of Integration for HRSL (solid line), SLSI (dashed line), SLEX (broken line) and FDEX (dotted line).

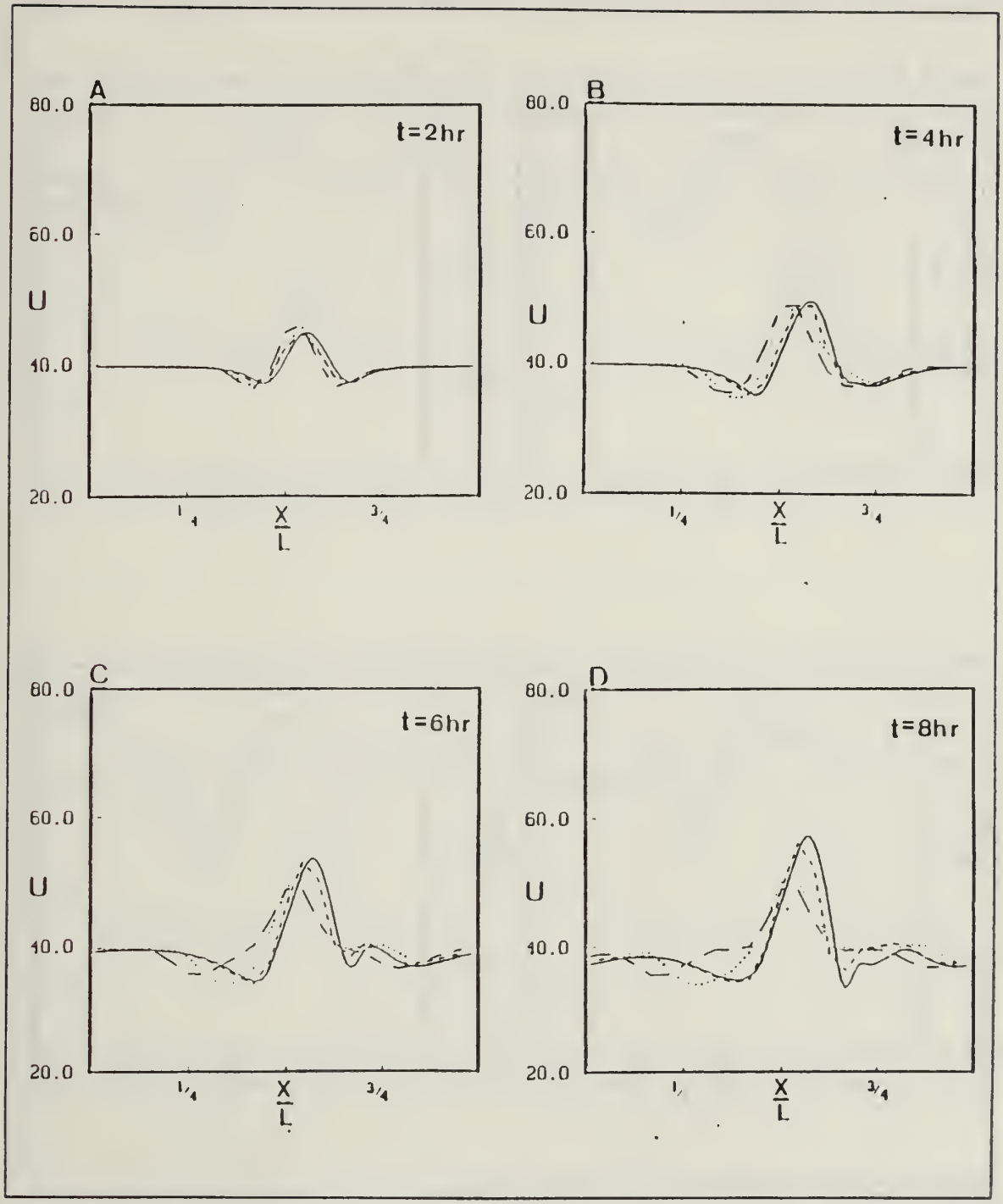

Figure 9. Experiment I, Case II: Total *u* Field (*m/s*) after A) Two B) Four C) Six D) Eight Hours of Integration for HRSL (solid line), SLSI (dashed line), SLEX (broken line) and FDEX (dotted line).

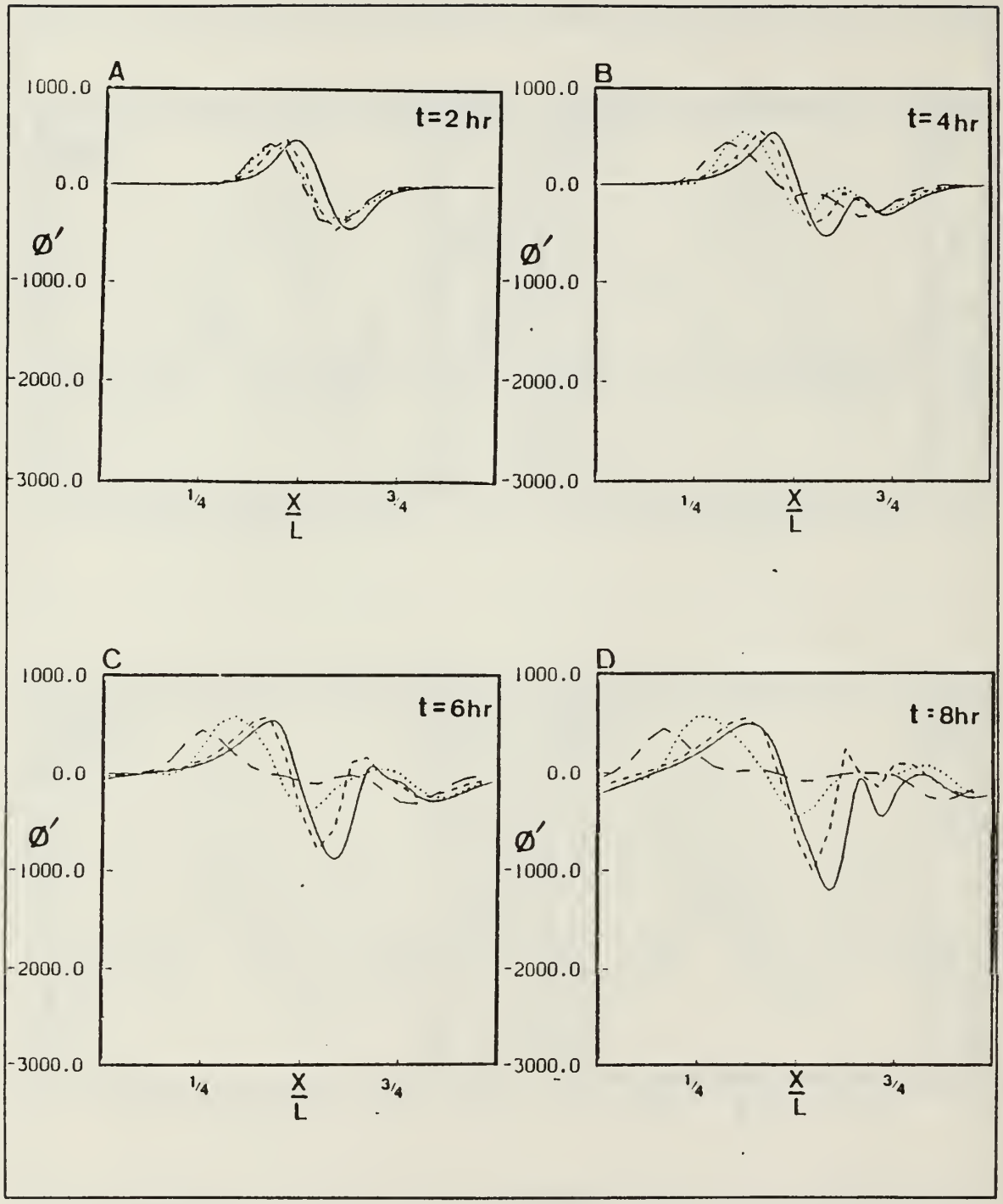

Figure 10. Experiment 1, Case II: ϕ' Field $(m/s)^2$ after A) Two B) Four C) Six D) Eight Hours of Integration for HRSL (solid line), SLSI (dashed line), SLEX (broken line) and FDEX (dotted line).

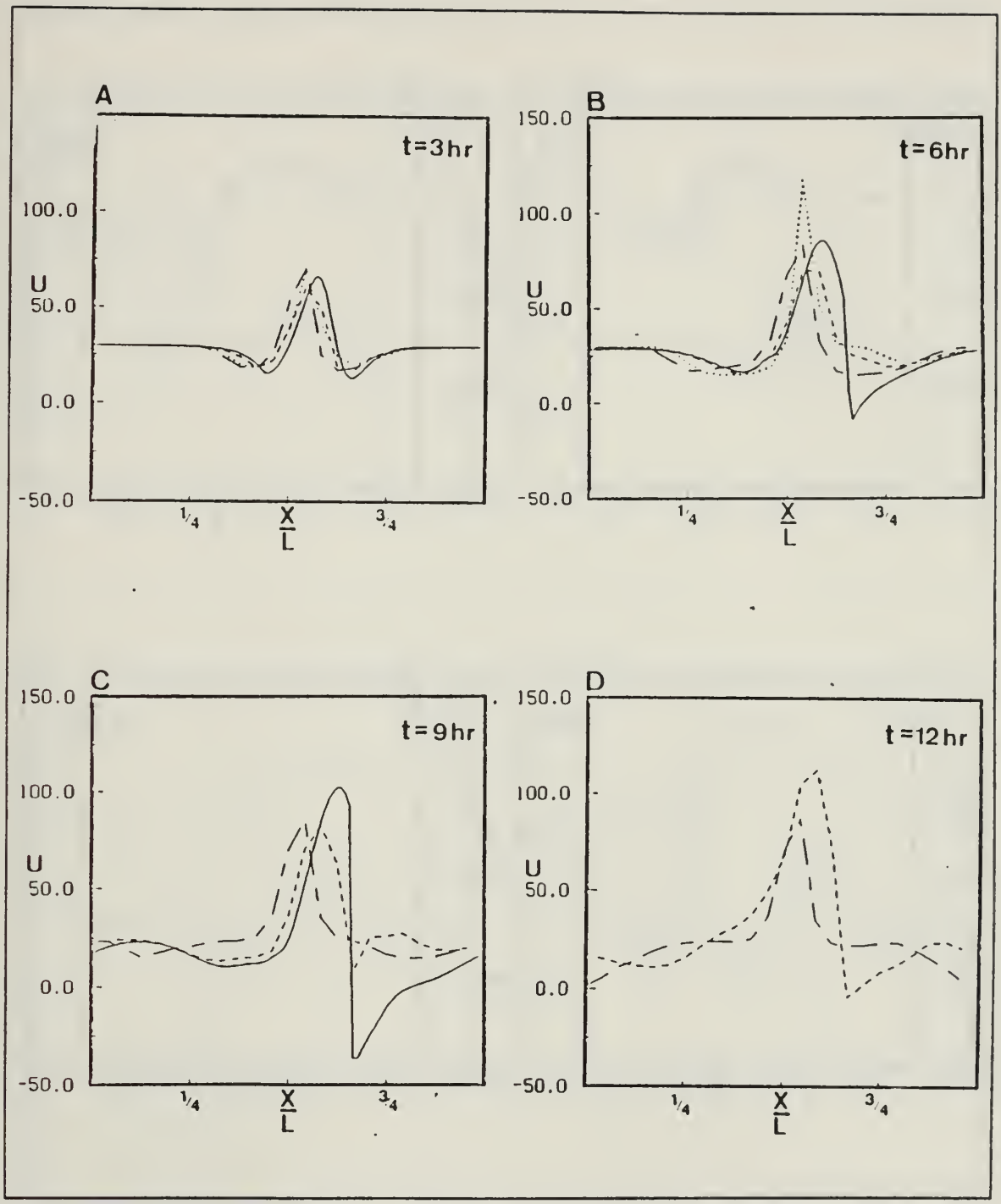

Figure 11. Experiment 1, Case III: Total *u* Field (*m/s*) after A) Two B) Four C) Six D) Eight Hours of Integration for HIRSL (solid line), SLSI (dashed line), SLEX (broken line) and FDEX (dotted line).

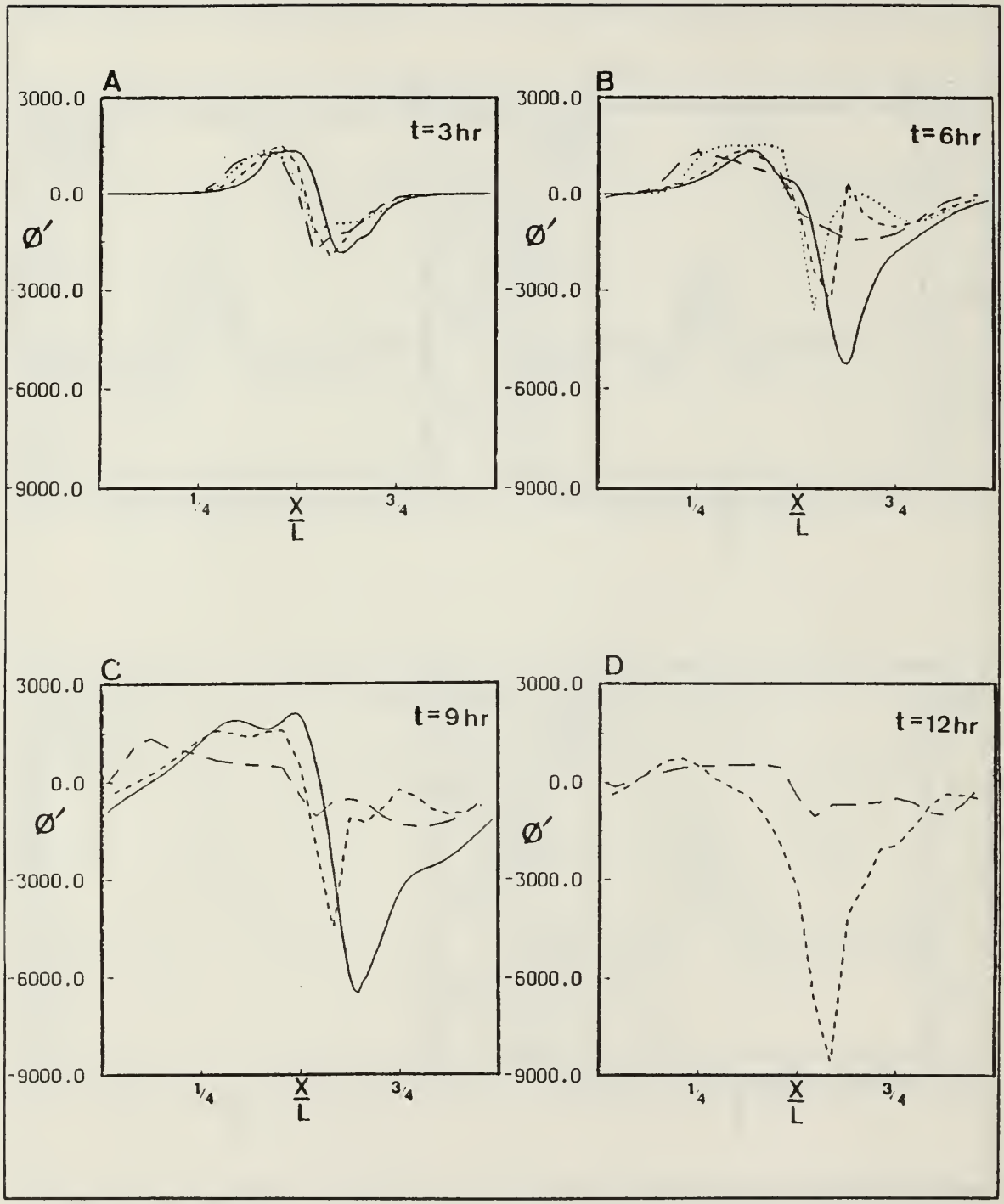

Figure 12. Experiment 1, Case III: ϕ' Field $(m/s)^2$ after A) Two B) Four C) Six D) Eight Hours of Integration for HRSL (solid line), SLSI (dashed line), SLEX (broken line) and FDEX (dotted line).

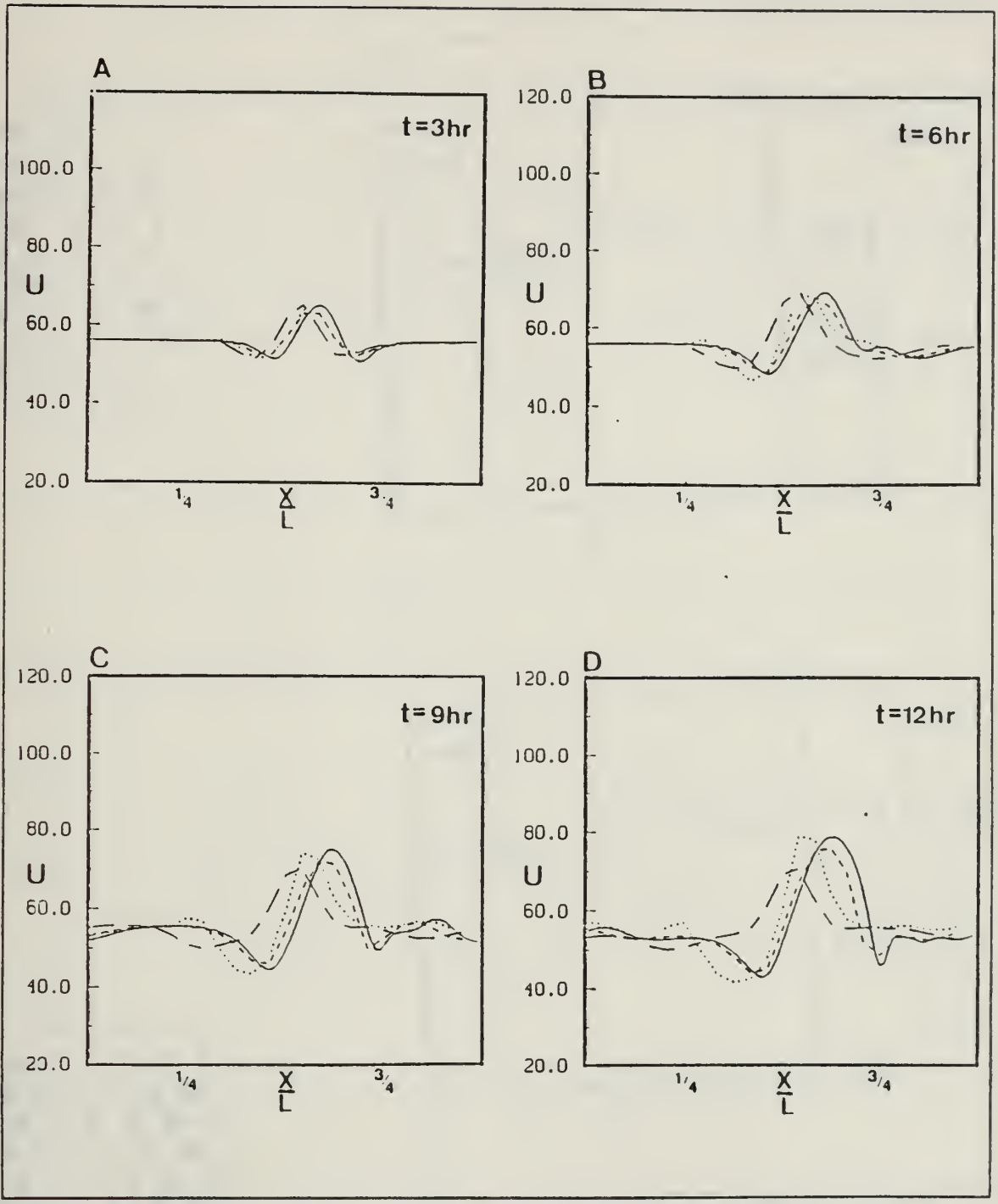

Figure 13. Experiment 1, Case IV: Total u Field (m/s) after A) Two B) Four C) Six D) Eight Hours of Integration for HRSL (solid line), SLSI (dashed line), SLEX (broken line) and FDEX (dotted line).

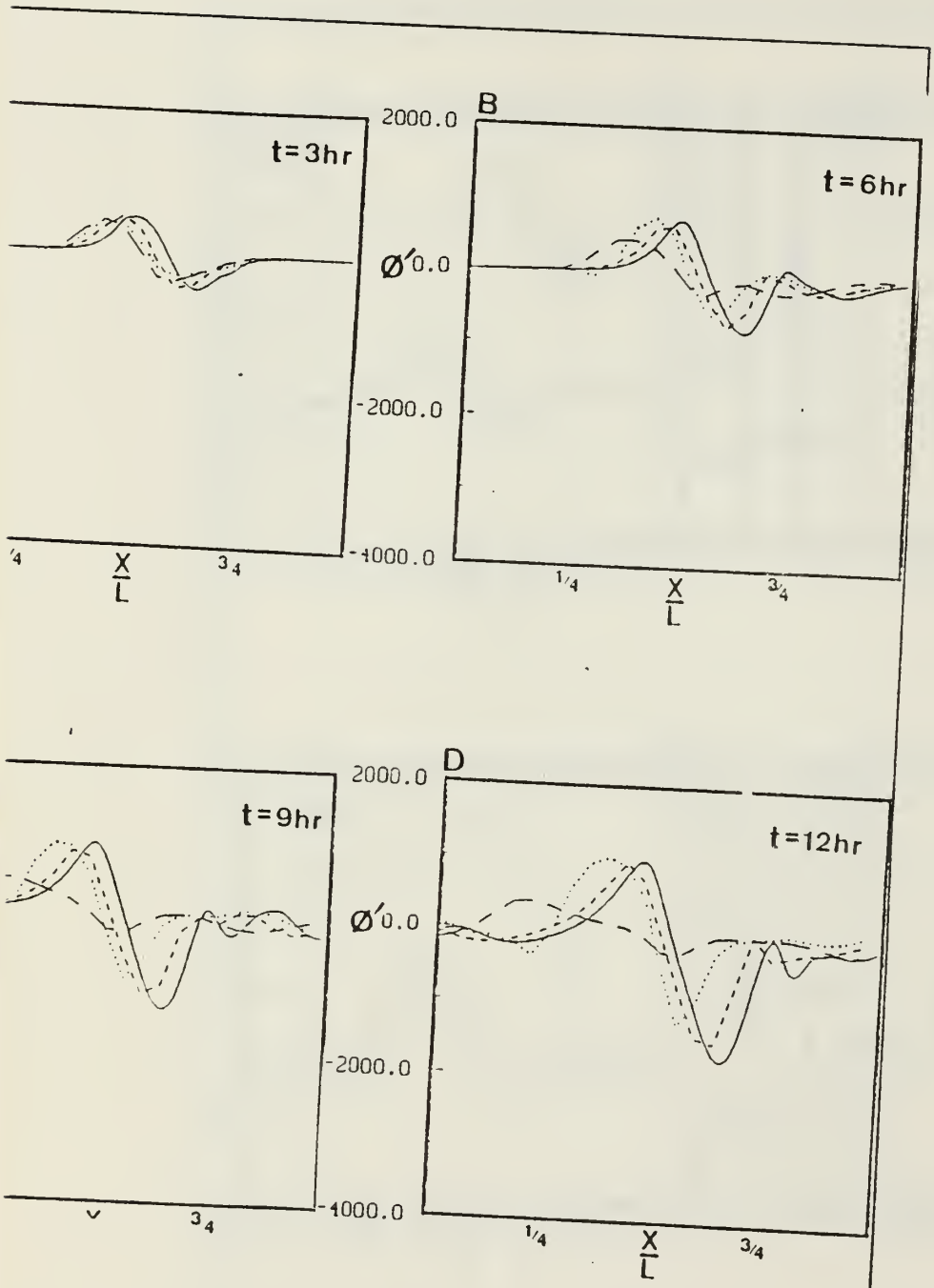

iment I, Case IV: ϕ' Field $(m/s)^2$ after A) Two B) Four C) Six
of Integration for HRSL (solid line), SLSI (dashed line), SLEX
FDEX (dotted line).

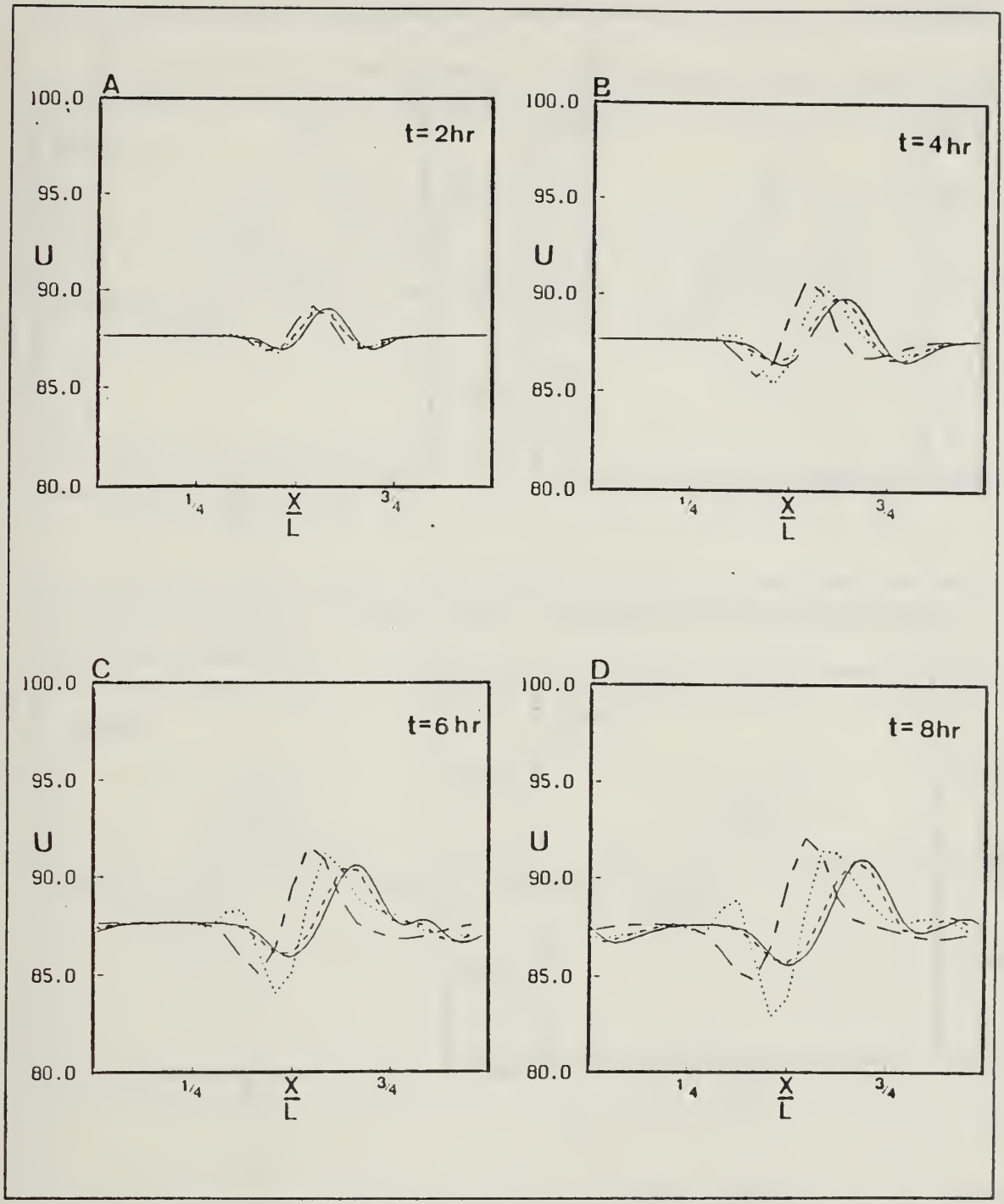

Figure 15. Experiment 1, Case V: Total *u* Field (*m/s*) after A) Two B) Four C) Six D) Eight Hours of Integration for HRSL (solid line), SLSI (dashed line), SLEX (broken line) and FDEX (dotted line).

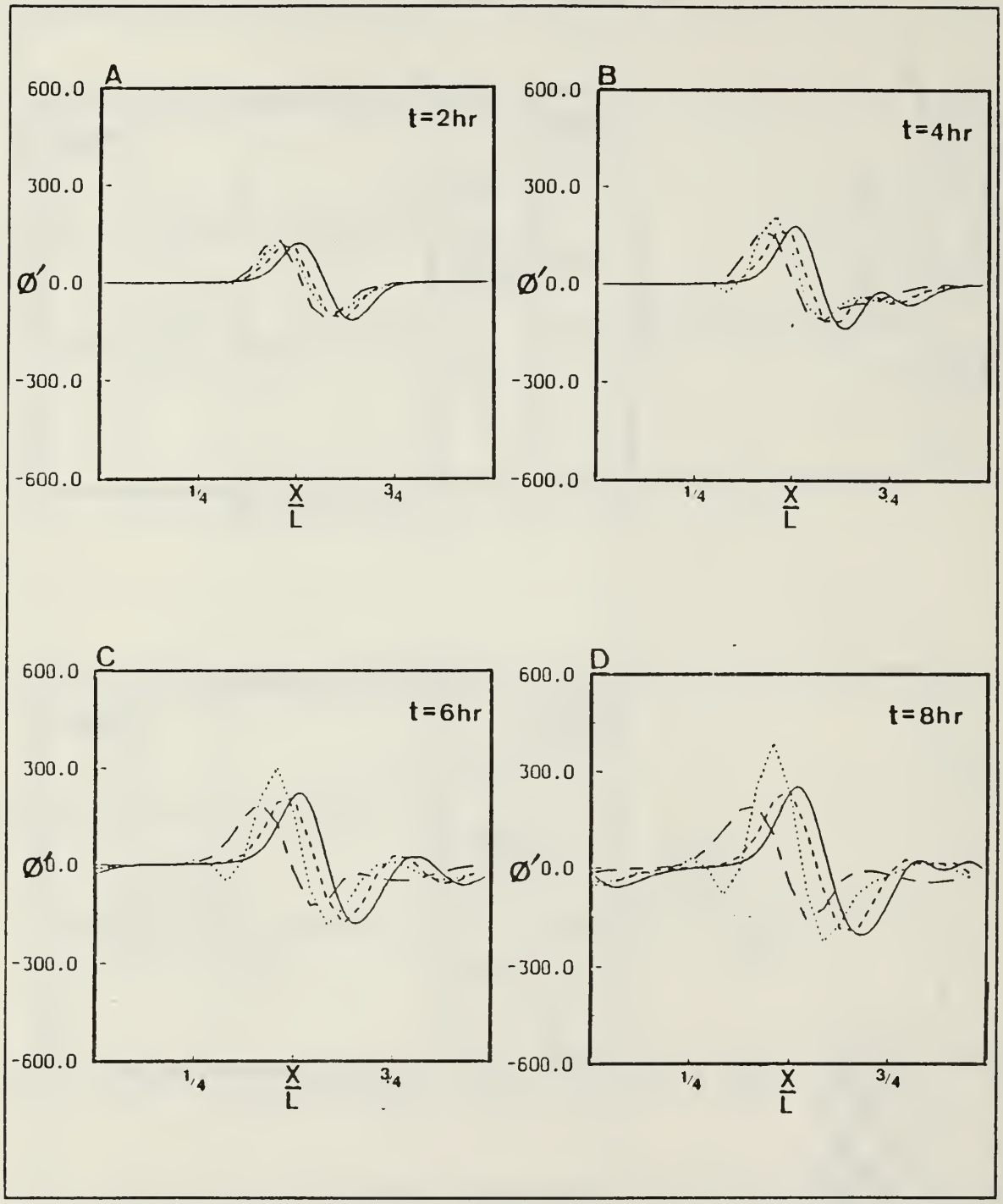

Figure 16. Experiment 1, Case V: ϕ' Field $(m/s)^2$ after A) Two B) Four C) Six D) Eight Hours of Integration for HRSL (solid line), SLSI (dashed line), SLEX (broken line) and FDEX (dotted line).

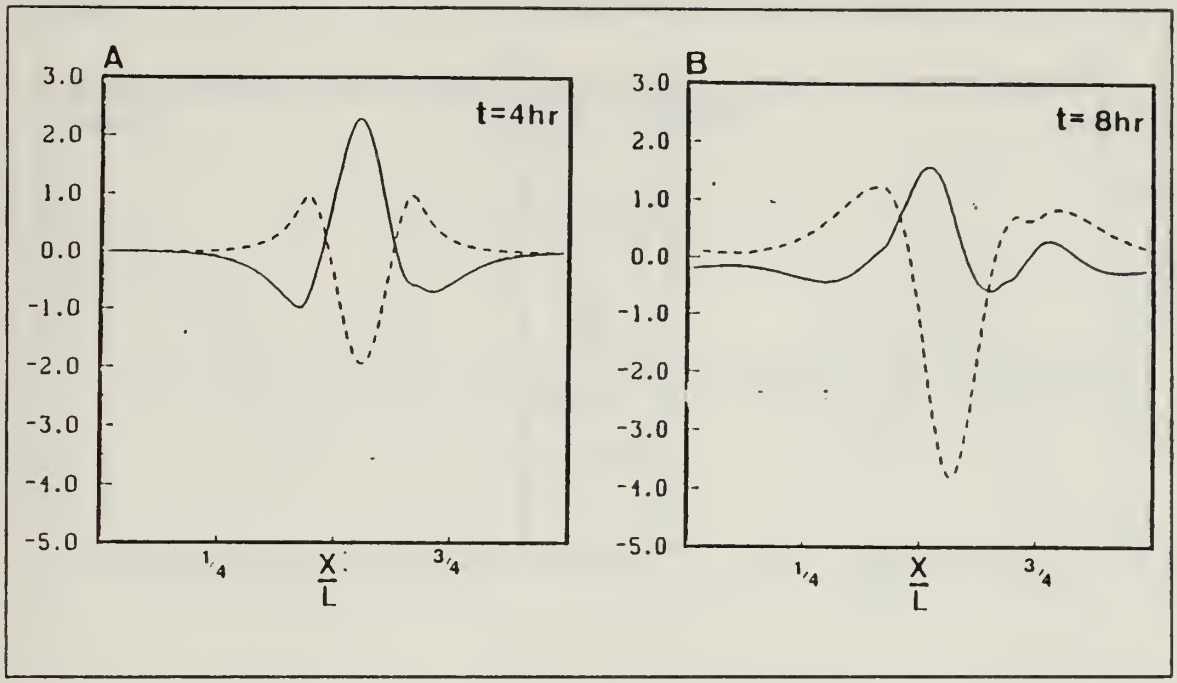

Figure 17. Experiment 2, Case I: u' and v' (m/s) after A) Four B) Eight Hours of Integration with HRSL.

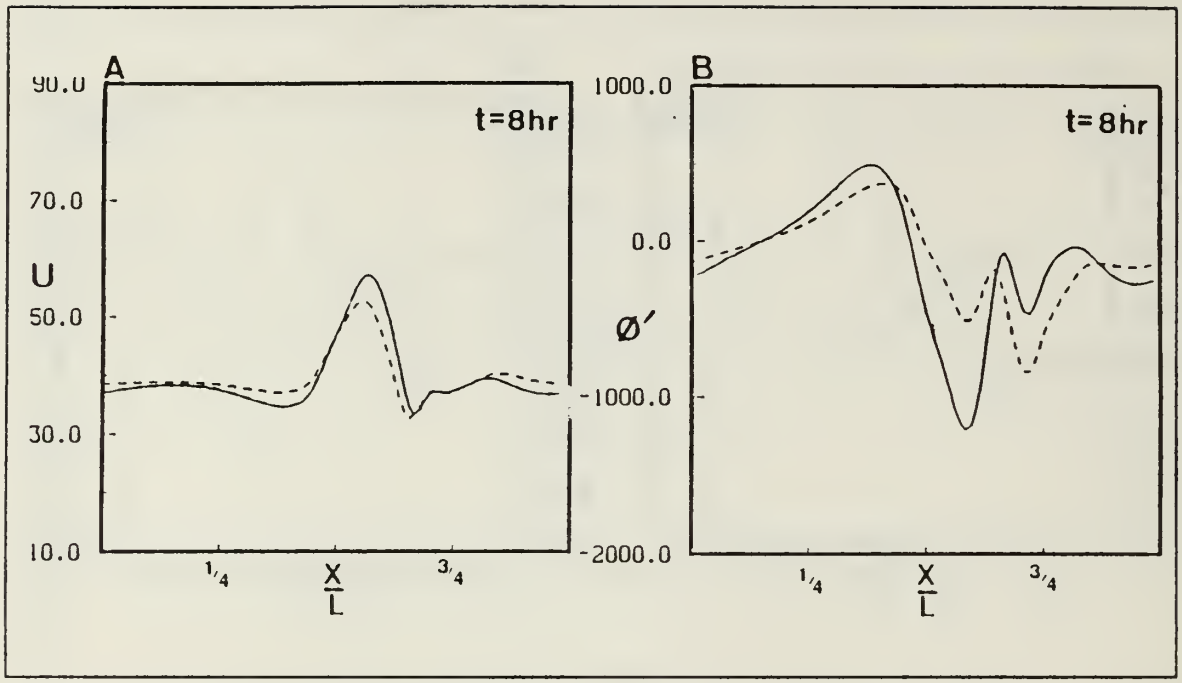

Figure 18. Comparison of Perturbations in Rotating and Non-rotating System $(m/s)^2$ for Case II A) u and B) ϕ' with HRSL. Solid line indicates non-rotating system; the dashed line indicates solution for the rotating system.

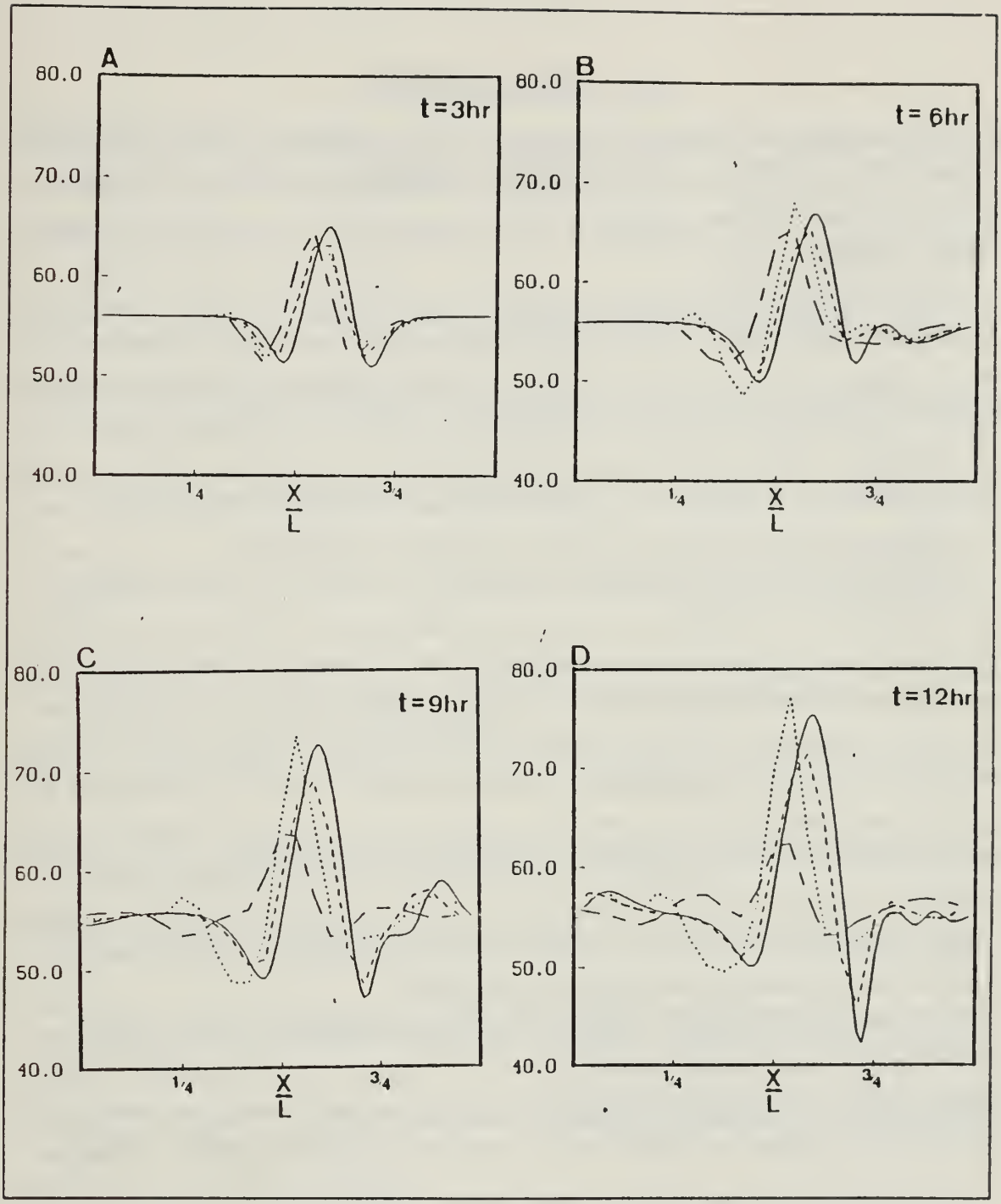

Figure 19. Experiment 2, Case IV: Total *u* Field (*m/s*) after A) Two B) Four C) Six D) Eight Hours of Integration for HRSL (solid line), SLSI (dashed line), SLEX (broken line) and FDEX (dotted line).

V. CONCLUSIONS

This investigation is a direct comparison of a semi-Lagrangian, semi-implicit model to the semi-Lagrangian, explicit and leapfrog finite difference models for the shallow water system with bottom topography. Of particular interest is the models' ability to simulate hydrolaulic jumps.

In the first experiment, the Coriolis parameter is set to zero, and the cases which Petroliagis (1988) examined with a Galerkin finite element model are reconstructed, albeit on a larger domain. Initially, the flow was uniform and zonal, and the free surface was flat. According to the theory of Houghton and Kasahara (1968), the first two cases are subcritical. A stable speed maximum should appear over the ridge. The last case is supercritical, and a speed minimum should develop over the ridge. The remaining cases are unstable and should produce a jump in the vicinity of the obstacle.

The SLSI forecasts are superior to the FDEX and SLEX forecasts for all cases. SLEX forecasts are destroyed by excessive smoothing due to interpolations; FDEX breaks down when the non-linear interaction become too large. SLSI results, however, are consistent with hydraulic jump theory. In the no jump cases, it forecasts stable speed and pressure maxima and minima where they are predicted by theory. SLSI forecasts increasing winds and dropping pressure for the jump cases. However, the details of the hydraulic jump which forms in case III are only apparent when the resolution is increased, and in Case IV, the domain is too small for a hydraulic jump to form before interference from the transient solutions due to the cyclic boundary conditions occurs. Further testing should be done on a larger domain (more isolated ridge) with the higher resolution semi-Lagrangian, semi-implicit model, HRSL.

In the second experiment, the same cases were re-examined, but the Coriolis parameter for 45°N was used to examine the effect of rotation on jump formation. Clearly, rotation slightly suppresses the perturbations in the free surface and delays the formation of hydraulic jumps, but further study is necessary for a more quantitative analysis.

LIST OF REFERENCES

Arakawa, A., and V.R. Lamb, 1977: Computational design of the basic dynamical processes of the UCLA general circulation model, *Methods in Computational Physics, Vol. 17,* Academic Press, 174-265, 337 pp.

Fjørtoft, R., 1952: On a numerical method of integrating the baratropic vorticity equation. *Tellus,* 8, 179-184.

Haltiner, G.J., and R.T. Williams, 1980: Numerical Prediction and Dynamic Meteorology. John Wiley & Sons, Inc., 477 pp.

Houghton, D.D. and A. Kasahara, 1968: Nonlinear shallow fluid flow over an isolated ridge. *Comm. Pure Appl. Math.,* 21, 1-23.

Kuo, H.-C., and R.T. Williams, 1989: Semi-Lagrangian solution to the Inviscid Burger equation. Submitted to the *Mon. Wea. Rev.*

Petroliagis, T.I., 1988: Studies of baratropic Flow over topography using a Galerkin finite element model. M.S. thesis, Naval Postgraduate School, Monterey, CA, 175 pp.

Pudykiewicz, J. and A. Staniforth, 1984: Some properties and comparitive performance of the semi-Lagrangian method of Robert in the solution of the advection-diffusion equation. *Atoms,-Ocean,* 22, 283-308.

Ritchie, H., 1987: Semi-Lagrangian advection on a gaussian grid. *Mon. Wea. Rev.,*155, 608-619.

Robert, A., 1981: A stable numerical integration scheme for the primitive meteorological equations. *Atmos-Ocean,*19, 35-46.

Sawyer, J.S., 1963: A semi-Lagrangian method of solving the vorticity advection equation. *Tellus,*15, 336-342.

Staniforth, A. and C. Temperton, 1986: Semi-implicit semi-Lagrangian intergration schemes for a barotropic finite-element regional model. *Mon. Wea. Rev.,*114, 2078-2090.

Wiin-Nielsen, A., 1959: On the Application of trajectory methods in numerical forecasting. *Tellus,* 11, 180-196.

Williams, R.T. and A.M. Hori, 1970: Formation of hydraulic jumps in a rotating system. *J. Geophys. Res.,* 75, 2813-2821.

INITIAL DISTRIBUTION LIST

		No. Copies
1.	Defense Technical Information Center Cameron Station Alexandria, VA 22304-6145	2
2.	Library, Code 0142 Naval Postgraduate School Monterey, CA 93943-5002	2
3.	Commander Naval Oceanography Command Stennis Space Center, MS 39529-5000	1
4.	Commanding Officer Naval Oceanography Office Stennis Space Center, MS 39529-5001	1
5.	Commanding Officer Naval Ocean Research and Development Activity Stennis Space Center, MS 39529-5004	1
6.	Commanding Officer Fleet Numerical Oceanography Center Monterey, CA 93943-5005	1
7.	Commanding Officer Air Force Global Weather Center Offutt Air Force Base, NE 68113	1
8.	Officer-in-Charge Naval Environment Prediction Research Facility Monterey, CA 93943-5006	1
9.	Prof. R.J. Renard, (Code 63Rd) Department of Meteorology Naval Postgraduate School Monterey, CA 93943-5000	1
10.	USAF ETAC/LD Air Weather Service Technical Library Scott Air Force Base, Illinois 62225	1
11.	Professor Roger T. Williams (Code 63Wu) Department of Meteorology Naval Postgraduate School Monterey, CA 93943-5000	5

12.	Professor Beny Neta (Code 53Nd) Department of Mathematics Naval Postgraduate School Monterey, CA 93943-5000	5
13.	Lieutenant Kristina B. Monk AFGWS/SDDN Offutt AFB, NE 68113	2
14.	Commanding Officer Naval Environmental Prediction Research Facility Monterey, CA 93943-5006	1
15.	Director Naval Oceanography Division Naval Observatory 34th and Massachusetts Avenue NW Washington, DC 20390	1
16.	Chairman, Oceanography Department U.S. Naval Academy Annapolis, MD 21402	1
17.	Chief of Naval Research 800 N. Quincy Street Arlington, VA 22217	1
18.	Office of Naval Research (Code 420) Naval Ocean Research and Development Activity 800 N. Quincy Street Arlington, VA 22217	1
19.	Library Acquisitions National Center for Atmospheric Research P.O. Box 3000 Boulder, CO 80307-5000	1
20.	Meteorology Reference Center, (Code 63) Department of Meteorology Naval Postgraduate School Monterey, CA 93943-5000	1
21.	Commander Air Weather Service Scott AFB, IL 62225	1
22.	Dr. Paul Twitchell Office of Naval Research 800 N. Quincy Street Arlington, VA 22217-5000	1
23.	Dr. T. Rosmond Naval Enviromental Prediction Research Facility Monterey, CA 93943-5000	1

24. Professor R.L. Elsberry (Code 63Es) 1
Department of Meteorology
Naval Postgraduate School
Monterey, CA 93943-5000

25. Professor A.L. Schoenstadt (Code 53Zh) 1
Department of Mathematics
Naval Postgraduate School
Monterey, CA 93943-5000

26. Professor R.E. Newton (Code 53Zh) 1
Department of Mechanical Engineering
Naval Postgraduate School
Monterey, CA 93943-5000

27. Professor M.A. Rennick (Code 63Rn) 1
Department of Meteorology
Naval Postgraduate School
Monterey, CA 93943-5000

28. Dr. J. Steppeler
European Center for Medium Range Weather Forecasts 1
Shinfield Park
Reading, Berkshire RG2 9AX
England

29. Dr. M.J.P. Cullen 1
Meteorology Office
Bracknell, Berks, United Kingdom
Pentagon
Washington, D.C. 20350-1000

30. Dr. Robert L. Lee 1
Atmospheric and Geophysical Science Division
University of California
P.O. Box 808
Livermore, CA 94550

31. Dr. Y. Sasake 1
Department of Meteorology
University of Okalahoma
Norman, OK 73069

32. Dr. Andrew Staniforth 1
Recherce-en-Previson Numerique
West Isle Office Tower, 5 ieme etage
2121 route Trans-Canada
Dorval, Quebec H9P1J3, Canada

33. Professor O.C. Zienkiewicz 1
Head of Civil Engineering Department
Applied Science Building
Singleton Park
Swansea SA2 8PP
United Kingdom

34. Captain M.D. McAtee 1
AFGWS/SDDN
Offutt AFB, NE 68113-0000